SEDIMENTOLOGY the journal of the International Association of Sedimentologists

Sedimentology (2014) **61**, 291–318 doi: 10.1111/sed.12095

Sedimentological and geochemical characteristics of a fluvial travertine: A case from the eastern Mediterranean region

MEHMET ÖZKUL*, ALİ GÖKGÖZ*, SANDOR KELE†, MEHMET ORUÇ BAYKARA*, CHUAN-CHOU SHEN‡, YU-WEI CHANG‡, ALİ KAYA*, METE HANÇER*, CİHAN ARATMAN*, TAYLAN AKIN* and ZEYNEP ÖRÜ§

**Department of Geological Engineering, Pamukkale University, TR–20070, Denizli, Turkey (E-mail: mozkul@pau.edu.tr)*

†Hungarian Academy of Sciences, Research Centre for Astronomy and Earth Sciences, Institute for Geological and Geochemical Research, Budaörsi út 45, H-1112 Budapest, Hungary

‡High-precision Mass Spectrometry and Environment Change Laboratory (HISPEC), Department of Geosciences, National Taiwan University, Taipei 10617 Taiwan

§Department of Geological Engineering, Istanbul University, Avcılar, Istanbul 34850 Turkey

Associate Editor – Enrico Capezzuoli

ABSTRACT

A sedimentological and geochemical study was performed on the travertines in the southern part of the Uşak geothermal field, western Turkey, to assess the applicability of a fluvial tufa facies model in interpreting late Quaternary travertine deposits developed along the stream valleys that follow fault and fracture systems. Modern thermal (31 to 38°C) springs are found on the floor of the valley between 480 m and 520 m above sea-level. The distribution and nature of travertine facies were determined from natural outcrops. Samples of the travertines and spring water were characterized using a range of geochemical and petrographic methods. Waterfall, slope and pool facies associations consist of various combinations of travertine facies and subordinate detrital facies. Waterfall and slope facies associations of the older deposits occur where the springs emerged onto a hillslope or topographic break. In contrast, the pool facies association developed in depressions or flat areas that were fed by thermal springs. The youngest generation (1·85 ka) precipitated at lower elevations than the older ones (147 to 153 ka). Stable carbon and oxygen isotope values of the Aksaz travertines range between +4·3‰ and +6·3‰ (Vienna Pee Dee Belemnite) and −12·6‰ and −7·2‰ (Vienna Pee Dee Belemnite), respectively. The high $\delta^{13}C$ values suggest that the thermal waters were charged with isotopically heavy CO_2 of deep origin. Based on palaeotemperature calculations, the temperatures of the palaeosprings are slightly higher (up to 44°C) than the present equivalents, but sometimes the temperature is lower, probably due to mixing with the stream water. Although the thermal waters occasionally are impeded by fluvial activity, travertine precipitation occurs in the protected parts of the Aksaz Stream valley. This contribution highlights the applicability of the fluvial facies model for tufa for the interpretation of travertine deposits worldwide.

Keywords Aksaz, facies, fluvial travertine, geochemistry, Uşak, western Turkey.

INTRODUCTION

Spring carbonates precipitate in various depositional settings. Based on field evidence, there is no single classification scheme overarching all spring carbonates (for example, tufa and travertine; Jones & Renaut, 2010; Capezzuoli *et al.*, 2013; this issue). For tufa deposits, freshwater carbonate developed under ambient temperature conditions, five depositional models were proposed by Ford & Pedley (1996) depending on outcrop-scale: (i) perched springline; (ii) cascade; (iii) fluvial; (iv) lacustrine; and (v) paludal. These models were based on the geometry and profile details, together with information on typical bed associations and characteristic facies (Pedley, 2009).

On the other hand, depositional models proposed for travertines (hydrothermal origin) are quite different. Based on geomorphology and depositional environment, Chafetz & Folk (1984) and Altunel & Hancock (1993) used the following terms for travertines in their studies: (i) terraced-mound travertine; (ii) fissure ridge travertine; (iii) range-front travertine; (iv) eroded-sheet travertine; (v) cascade travertine; and (vi) self-built channel travertine. More recently Guo & Riding (1998) suggested an alternative classification scheme using the depositional systems of the travertine deposits occurring at Rapolano Terme (central Italy): (i) slope; (ii) depression; and (iii) mound depositional systems.

Among the tufa models, the fluvial barrage model is the most common one described for different climatic zones, including cool temperate, warm semi-arid, arid and seasonally wet tropical settings (Ford & Pedley, 1996; Arenas *et al.*, 2000; Carthew *et al.*, 2003, 2006; Viles *et al.*, 2007; Pedley, 2009; Vázquez-Urbez *et al.*, 2012). The fluvial model, which was proposed for tufa, occurs along a karstic valley (Ford & Pedley, 1996) and excludes spring systems where deposits (travertine) formed from a hot-water springs scheme (Jones & Renaut, 2010).

The depositional setting of the Aksaz travertines, near Ulubey, south of Uşak, Western Turkey (Fig. 1), cannot be explained precisely using existing morphological and depositional models (Chafetz & Folk, 1984; Altunel & Hancock, 1993; Guo & Riding, 1998). These travertines were precipitated along an ephemeral stream valley running to the south-west, which is incised into a narrow tectonic lineament damage zone (i.e. fault and/or fracture). These damage zones play an important role in the circulation and upwelling of hydrothermal fluids in geothermal areas (Hancock *et al.*, 1999; Uysal *et al.*, 2007; Brogi & Capezzuoli, 2009; De Filippis *et al.*, 2012; Van Noten *et al.*, 2013). Consequently, on a large scale, the depositional setting of the Aksaz travertines resembles the present fluvial model proposed for tufa deposits (Pedley, 1990, 2009; Ford & Pedley, 1996; Arenas-Abad *et al.*, 2010; Vázquez-Urbez *et al.*, 2012).

In this study, for the first time, a fluvial model, which originally was suggested only for tufa deposits, is applied to clarify the depositional setting of the Aksaz travertines. For this purpose, depositional and geochemical properties are described and a fluvial model is proposed to be applied worldwide to travertine resulting from hot-water springs, as well as tufa.

GEOLOGICAL SETTING

The north-east-trending Uşak-Güre basin, in the western extensional province of Turkey, was initiated during the Early Miocene (Seyitoğlu, 1997; Fig. 1). The basin fill is underlain by the basement rocks of the Menderes Massif that covers a significant portion of western Turkey, and includes variable grade metamorphic rocks (i.e. gneiss, schist, marble and quartzite) and young granitoid intrusions (Bozkurt & Park, 1994; Hetzel *et al.*, 1995; Gessner *et al.*, 2001). The basement rocks of the Uşak-Güre basin consist mainly of marbles and schists. This Neogene basin fill was divided into two groups by Ercan *et al.* (1978, 1983). The basal Hacıbekir Group is composed of alluvial, fluvial and lacustrine sediments and associated coeval volcanics. The Hacıbekir Group is cut by 18·9 ± 0·6 Ma (Early Miocene) volcanics (Seyitoğlu, 1997) and is unconformably overlain by the İnay Group, which is formed mainly of lacustrine sediments with marginal alluvial deposits. These strata interfinger with volcanic strata. The Hacıbekir Group, dated both isotopically and by the Eskihisar sporomorph association (20 to 14 Ma), is older than 14 Ma (Seyitoğlu, 1997; Seyitoğlu *et al.*, 1997). The Upper Miocene Asartepe Formation unconformably overlies the İnay Group, and the Kula volcanics cover all earlier basin fill (Seyitoğlu *et al.*, 2009). Additional isotopic age results from the volcanic rocks in the region confirm the stratigraphy of the Uşak–Güre basins (Innocenti *et al.*, 2005; Purvis *et al.*, 2005; Ersoy & Helvacı, 2007; Ersoy *et al.*, 2008, 2010).

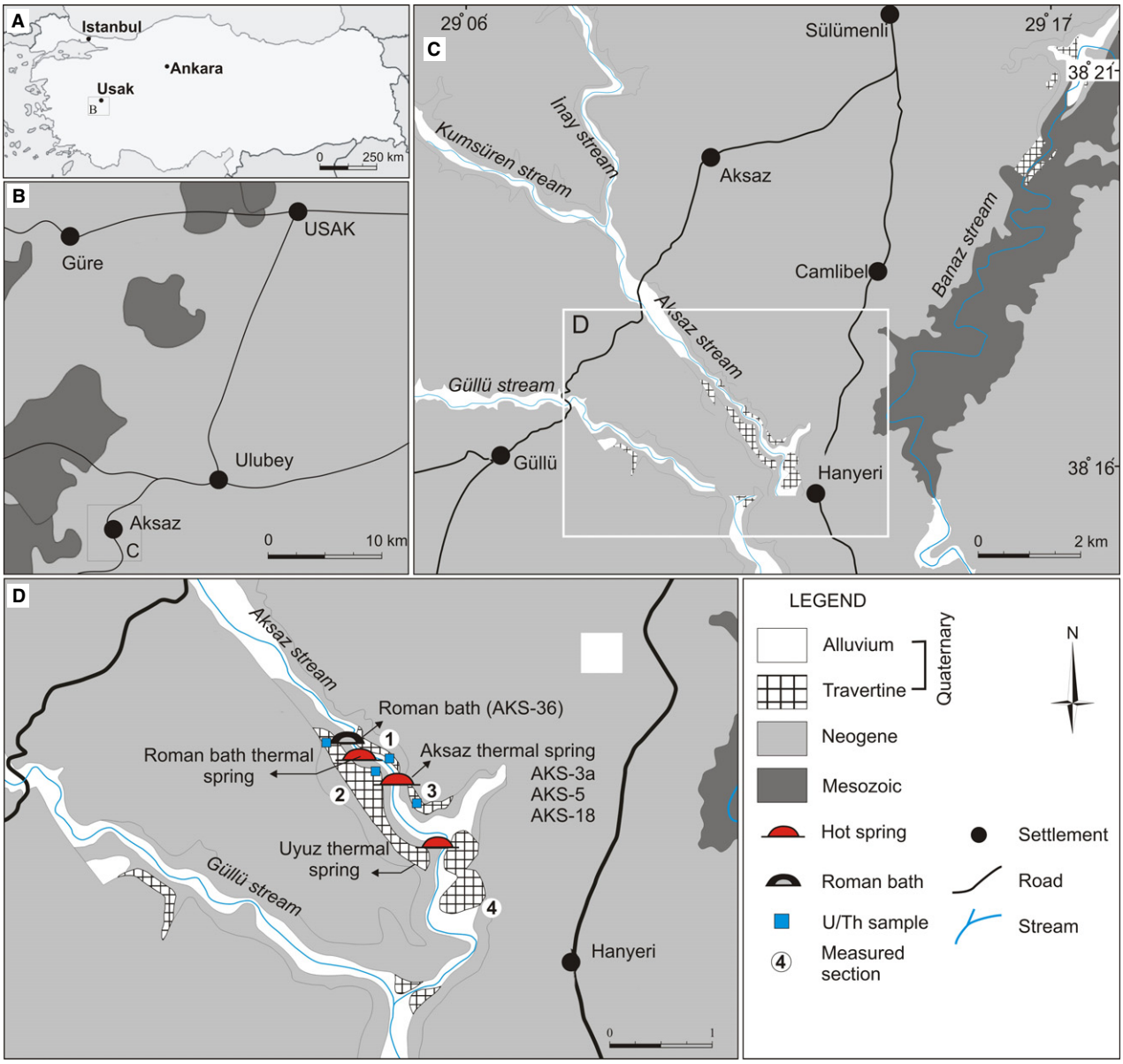

Fig. 1. (A) Geographical setting of Uşak province in Turkey. (B) Location of the Aksaz area in the Uşak province with basic rock units. (C) Travertine occurrences in fluvial settings along the NE and NW-trending stream beds following the tectonic lines (for example, faults and fractures). (D) Late Quaternary travertine occurrences studied and accompanying active hot springs located in the SE-trending Aksaz Stream valley. The locations of dated samples (AKS-3a, AKS-5, AKS-18 and AKS-36) are marked on the map. The encircled numbers indicate locations of the measured sections in Fig. 2.

Around Ulubey, in the southern part of the Uşak–Güre basin, western Turkey, the stream beds are mostly north-east and north-west-trending with most following faults and fractures, which are pathways for upwelling hydrothermal fluids (Hancock *et al.*, 1999; Şimşek, 2003; Brogi & Capezzuoli, 2009). In many of these stream valleys, travertine deposits have been precipitated from hydrothermal fluids (Fig. 1C and D).

Travertines are found along the Aksaz Stream, which is located to the south-west of Ulubey, in Uşak province (Fig. 1B to D). The stream has incised into the upper part of the Miocene fluvio-lacustrine succession and still flows towards the south-east. A borehole, drilled near Aksaz Spring, penetrated a 20 m thickness of Neogene sequence before reaching the Mesozoic marble.

SAMPLING AND ANALYTICAL METHODS

Fieldwork was carried out on natural travertine cliffs along the Aksaz Stream valley and quarry faces near the village of Hanyeri (Fig. 1). During the field study facies descriptions were performed, and samples were collected from the travertines and associated sediments. Additional sampling was performed on 28 November 2012 at a recent thermal seep, located 50 m downstream from the main Aksaz Spring (Fig. 1), in order to collect both recent travertine and water samples directly from the small spring orifice and the nearby stream bed.

For mineralogical, petrographical, geochronological and geochemical evaluation, 23 element analyses, 27 stable isotope measurements, four U-Th dating and 46 X-ray diffraction (XRD) analyses were performed on the collected samples. The 154 scanning electron microscope (SEM) images have been used to evaluate texture and microbial components. Scanning electron microscope and XRD analyses were performed at the Turkish Petroleum Corporation (TPAO) in Ankara, Turkey.

Samples were sputter coated with a very thin layer of gold before SEM analyses. Scanning electron microscope investigations were performed using a JEOL JSM 6490 LV (JEOL Limited, Tokyo, Japan). Mineralogical compositions of the samples were determined by an X-ray powder diffraction (XRD) technique using a Rigaku D/Max–2200 diffractometer (Rigaku Corporation, Tokyo, Japan) with CuKα radiation at 40 kV and 20 mA. A semi-quantitative phase analysis was made on randomly oriented powdered samples. The relative error of the quantification is 5 to 10%.

Elemental measurements of the water and travertine samples from different sites were carried out at the Acme Analytical Laboratory (ACMELAB, Vancouver, Canada), using the inductively coupled plasma mass spectrometer (ICP-MS) technique. The ion content of the waters was determined using a Dionex ICS 1000 ion chromatography instrument (Dionex Corp., Sunnyvale, CA, USA) at Pamukkale University in Denizli. Calcite saturation indices of the waters were calculated using the PHREEQC computer program (Parkhurst & Appelo, 1999). The stable isotope values of the thermal waters were measured at the stable isotope ratio facility for environmental research (SIRFER) at the University of Utah (USA), using Thermo Finnigan Delta Plus XL Isotope Ratio Mass Spectrometer (Thermo Fisher Scientific Inc., Bremen, Germany).

Stable carbon and oxygen isotope measurements of the travertine (25 old and one recent) and one additional water sample that was taken subsequently were performed at the Institute for Geological and Geochemical Research, Hungarian Academy of Sciences, Budapest, Hungary. Carbon and oxygen isotope analyses of bulk travertine samples were carried out using both the conventional phosphoric acid method (H_3PO_4 digestion method at 25°C) of McCrea (1950) and the continuous flow technique of Spötl & Vennemann (2003). $\delta^{18}O$ analyses of waters were conducted using the CO_2–water equilibration method of Epstein & Mayeda (1953). Hydrogen isotope compositions were determined on water samples using the H_2O–Zn reaction method (Coleman *et al.*, 1982; Kendall & Coplen, 1985; Demény, 1995) and Pt-assisted H_2–H_2O equilibration (Coplen *et al.*, 1991; Prosser & Scrimgeour, 1995). $^2H/H$, $^{13}C/^{12}C$ and $^{18}O/^{16}O$ ratios were determined in H_2 and CO_2 gases using Finnigan MAT delta S and Thermo delta plus XP mass spectrometers (Thermo Fisher Scientific Inc., Bremen, Germany). All samples were measured at least in duplicate and the mean values are given in the standard δ notation in parts per thousand (‰) relative to Vienna Pee Dee Belemnite (VPDB; $\delta^{13}C$ and $\delta^{18}O$) and Vienna Standard Mean Ocean Water (VSMOW; $\delta^{18}O$ and δD). Reproducibilities are better than $\pm 0{\cdot}1$‰ for $\delta^{13}C$ and $\delta^{18}O$ values of carbonates, $\pm 0{\cdot}1$‰ for the $\delta^{18}O$ and ± 2‰ for δD values of waters.

Before the U-Th chemistry, selected travertine samples (compact, light-coloured and primary deposits) were crushed gently, treated ultrasonically, and dried. About 50 to 100 mg of each subsample was chosen for U-Th chemistry (Shen *et al.*, 2008) in a class-10,000 geochemical clean room with class-100 benches at the High-precision Mass Spectrometry and Environment Change Laboratory (HISPEC), Department of Geosciences, National Taiwan University. A triple-spike, ^{229}Th–^{233}U–^{236}U, isotope dilution method (Shen *et al.*, 2003) was employed to correct mass bias and determine U and Th isotopic and concentration data (Shen *et al.*, 2002). Measurements of U and Th isotopic abundances were performed on an inductively coupled plasma mass spectrometer (MC-ICPMS), Neptune (Thermo Fisher Scientific Inc., Bremen, Germany; Shen *et al.*, 2012). Uncertainties in

the U-Th isotopic data were calculated offline (Shen *et al.*, 2002) at the 2σ level, and include corrections for blanks, multiplier dark noise, abundance sensitivity and contents of the four nuclides in spike solution. ^{230}Th dates (yr BP, before 1950 AD; Table 1) were calculated using decay constants of $9{\cdot}1577 \times 10^{-6}$ yr^{-1} for ^{230}Th and $2{\cdot}8263 \times 10^{-6}$ yr^{-1} for ^{234}U (Cheng *et al.*, 2000) and $1{\cdot}55125 \times 10^{-10}$ yr^{-1} for ^{238}U (Jaffey *et al.*, 1971).

PRESENT HOT SPRINGS AND WATER GEOCHEMISTRY

Today, three thermal springs and several seepages discharge along the ephemeral Aksaz Stream which lies from 520 to 480 m above sea-level (a.s.l.). The Roman bath thermal spring is located 400 m upstream of the Aksaz Spring area, whereas the Uyuz thermal spring is *ca* 1 km downstream of the Aksaz Spring (Fig. 1). The thermal springs are submerged by the stream waters during the wet season, but lie above the water during the dry season. During the period from October 2008 to August 2010 the water temperature (*T*) was 31·1 to 37·6°C, electrical conductivity (EC) was 3860 to 4330 (μmho cm^{-1}) and the pH was 6·14 to 6·34 (Table 2). In December 2012, thermal water and recent travertine samples were collected from a seepage 50 m downstream of the Aksaz Spring. The *in situ* measured physicochemical parameters of water at the orifice of the sampled thermal spring were: T = 35·8°C; pH = 6·37; EC = 4110 μS cm^{-1}; and Eh = 35·8 mV.

The chemical compositions of the sampled springs and seep waters in the Aksaz area, upwelling from the Mesozoic marbles, were similar to one another. The element content of the spring waters was: Ca: 255 to 358 mg l^{-1}, Mg: 87 to 99 mg l^{-1}, HCO_3: 1326 to 1525 mg l^{-1}, SO_4: 1214 to 1324 mg l^{-1} (Table 2). Some element concentrations are remarkable such as B (5·55 to 6·48 mg l^{-1}), As (0·31 to 0·57 mg l^{-1}) and Sr (8·21 to 9·84 mg l^{-1}). The saturation levels with respect to calcite range from 0·16 to 0·35 and, consequently, the waters tend to precipitate travertine. The spring waters that are of Na–Ca–SO_4–HCO_3 type discharge mainly from three springs, one of the most prominent of which is the Aksaz Spring with a flow rate of 28 l sec^{-1} (Akkuş *et al.*, 2005).

The δ^{18}O and δD values of the thermal spring waters (for example, the Aksaz and Uyuz springs) during the same periods mentioned

Table 1. U-Th isotopic compositions and ^{230}Th ages for Aksaz travertine samples by MC-ICPMS, Thermo Fisher Neptune, at NTU.

Sample ID	Chem ID	^{238}U ppb	^{232}Th ppt	$\delta^{234}U_{measured}$*	$[^{230}Th/^{238}U]_{activity}$‡	$[^{230}Th/^{232}Th]_{activity}$	Age uncorrected	Age corrected‡,§	$\delta^{234}U_{initial}$ corrected†
AKS-3a	O1	430·58 ± 0·74	1071·4 ± 6·2	198·5 ± 2·6	0·91320 ± 0·00230	1121·6 ± 6·8	146 867 ± 1047	146 816 ± 1046	300·5 ± 4·1
AKS-5	O2	455·21 ± 0·67	208 ± 10	188·7 ± 2·4	0·92340 ± 0·00210	6182 ± 312	153 123 ± 1018	153 113 ± 1018	290·9 ± 3·7
AKS-18	O3	1082·7 ± 1·10	115·3 ± 5·5	131·6 ± 1·8	0·37027 ± 0·00066	10624 ± 511	42 914 ± 128	42 911 ± 128	148·6 ± 2·0
AKS-36	O4	507·23 ± 0·65	11609 ± 43	347·1 ± 2·2	0·02807 ± 0·00081	3·75 ± 0·11	2297 ± 67	1 848 ± 235	349·0 ± 2·2

Chemistry was performed on 7 April 2011 (Shen *et al.*, 2003) and instrumental analysis on MC-ICP-MS (Shen *et al.*, 2012). Analytical errors are 2σ of the mean. Decay constants are $9{\cdot}1577 \times 10^{-6}$ year^{-1} for ^{230}Th, $2{\cdot}8263 \times 10^{-6}$ year^{-1} for ^{234}U (Cheng *et al.*, 2000) and $1{\cdot}55125 \times 10^{-10}$ year^{-1} for ^{238}U (Jaffey *et al.*, 1971). *$\delta^{234}U = ([^{234}U/^{238}U]_{activity} - 1) \times 1000$. †$\delta^{234}U_{initial}$ corrected was calculated based on ^{230}Th age (T), i.e. $\delta^{234}U_{initial} = \delta^{234}U_{measured} \times e^{\lambda 234 * T}$ and T is corrected age. ‡$[^{230}Th/^{238}U]_{activity} = 1 - e^{-\lambda 230 T} + (\delta^{234}U_{measured}/1000)[\lambda 230/(\lambda 230 - \lambda 234)](1 - e^{-(\lambda 230 - \lambda 234)T})$, where T is the age. §Age corrections were calculated using an estimated activity ^{230}Th/^{232}Th ratio of 0·74 ± 0·37.

Table 2. The chemical and isotopic compositions of the Aksaz and Uyuz thermal springs and the Aksaz stream water (EC: μmho cm^{-1}, Eh: mV, ions in mg l^{-1}).

ID	Date	*T* °C	EC	pH	Eh	HCO_3	Cl	SO_4	Na	K	Ca	Mg	As	B	Sr	$\delta^{18}O$ (‰ VSMOW)	δD (‰ VSMOW)	*T* (TU)
Aksaz	October 2008	34·9	3860	6·38	41·3	1326	60	1214	585	88	346	87	–	–	–	−8·7	−63·8	0
	May 2009	37·0	4160	6·25	51·0	1440	69	1214	592	85	358	89	–	–	–	−9·2	−67·0	0
	August 2009	37·6	4330	6·34	53·8	1525	70	1256	585	80	348	92	–	–	–	–	–	–
	August 2010	37·6	4210	6·35	38·0	1480	80	1230	638	95	373	94	0·57	5·55	8·21	−9·4	−63·0	2·10
Uyuz	October 2008	31·5	3970	6·28	47·0	1326	54	1243	609	91	330	98	–	–	–	−8·9	−73·7	0
	May 2009	31·5	4040	6·15	56·2	1380	68	1309	583	86	255	95	–	–	–	−9·3	−65·0	0·16
	August 2009	31·1	4050	6·29	55·4	1390	69	1319	613	82	338	94	–	–	–	–	–	–
	August 2010	32·3	3960	6·14	49·5	1420	76	1324	614	92	313	99	0·31	6·48	9·84	−9·1	−64·0	1·41
Aksaz stream	October 2008	10·7	1426	7·59	−27·0	380	103	310	90	20	156	60	–	–	–	−6·4	−50·8	1·24
	February 2009	9·6	485	7·45	−19·0	160	24	75	24	7	46	17	–	–	–	–	–	–
	May 2009	18·9	1043	7·25	−6·6	362	68	141	77	17	93	37	–	–	–	−6·2	-42·0	–
	August 2009	30·8	4290	7·15	5·0	1525	73	1291	585	80	348	92	–	8·02	9·39	–	–	5·35

VSMOW, Vienna Standard Mean Ocean Water.

above varied from −9·4 to −8·7‰ and −73·7 to −63·0‰ (VSMOW), respectively. In December 2012, the $\delta^{18}O$ and δD values of the water samples from the Aksaz Spring were obtained as −9·2‰ and −71·1‰ (VSMOW), respectively, while the water sample collected from the adjacent streamwater had more positive values ($\delta^{18}O$: −6·2 to −6·4‰; δD: −42·0 to −50·8‰). These values, which correspond or are close to the global meteoric water line (Craig, 1961), indicate that the thermal waters are meteoric in origin. Tritium contents of the waters are between 0·00 and 2·10 TU (Tritium Unit), showing that the residence times are more than 50 years. According to silica geothermometer equations (Fournier, 1977), the reservoir temperature of the Aksaz geothermal field can reach up to 127°C. Previously, the reservoir temperatures for the Uşak geothermal waters were determined as up to 120°C (Davraz, 2008). The chemical composition of the Aksaz streamwater varies seasonally. For instance, the EC value was measured as 485 μmho cm^{-1} in February 2009, 1043 μmho cm^{-1} in May 2009 and 4290 μmho cm^{-1} in August 2009.

STRATIGRAPHY

Inactive travertines are exposed as cliffs on both sides of Aksaz Stream (Fig. 1C and D) at elevations between 450 m and 500 m a.s.l.. The fluvial deposits, which are represented by conglomerates, sandstones and mudstones, occur mainly at the lower parts of the travertine sequences (Fig. 2). The conglomerates are composed mainly of quartzite, schist, sandstone and marl derived from the metamorphic and Neogene sedimentary bedrocks. The travertine sections are 5 to 12 m thick in the Aksaz area and up to 24 m thick at Hanyeri (Fig. 2). U-Th age dating indicates that travertine deposition took place largely during MIS 6 (147 to 153 ka) and MIS 3 (43 ka; Table 1). The ^{232}Th levels are very low, only 100 to 1000 ppt for samples AKS-3a, AKS-5 and AKS-18, and 11609 ppt for sample AHS-36. Detrital contamination causes only 10 to 450 years of ageing (Table 1), using a $^{230}Th/^{232}Th$ atomic ratio of 4 ± 2 ppm, which is the value for material at secular equilibrium with the crustal $^{232}Th/^{238}U$ value of 3·8 and an arbitrarily assumed uncertainty of 50% (Taylor & McLennan, 1995).

Field observations indicate that travertine deposition, with time, migrated from higher

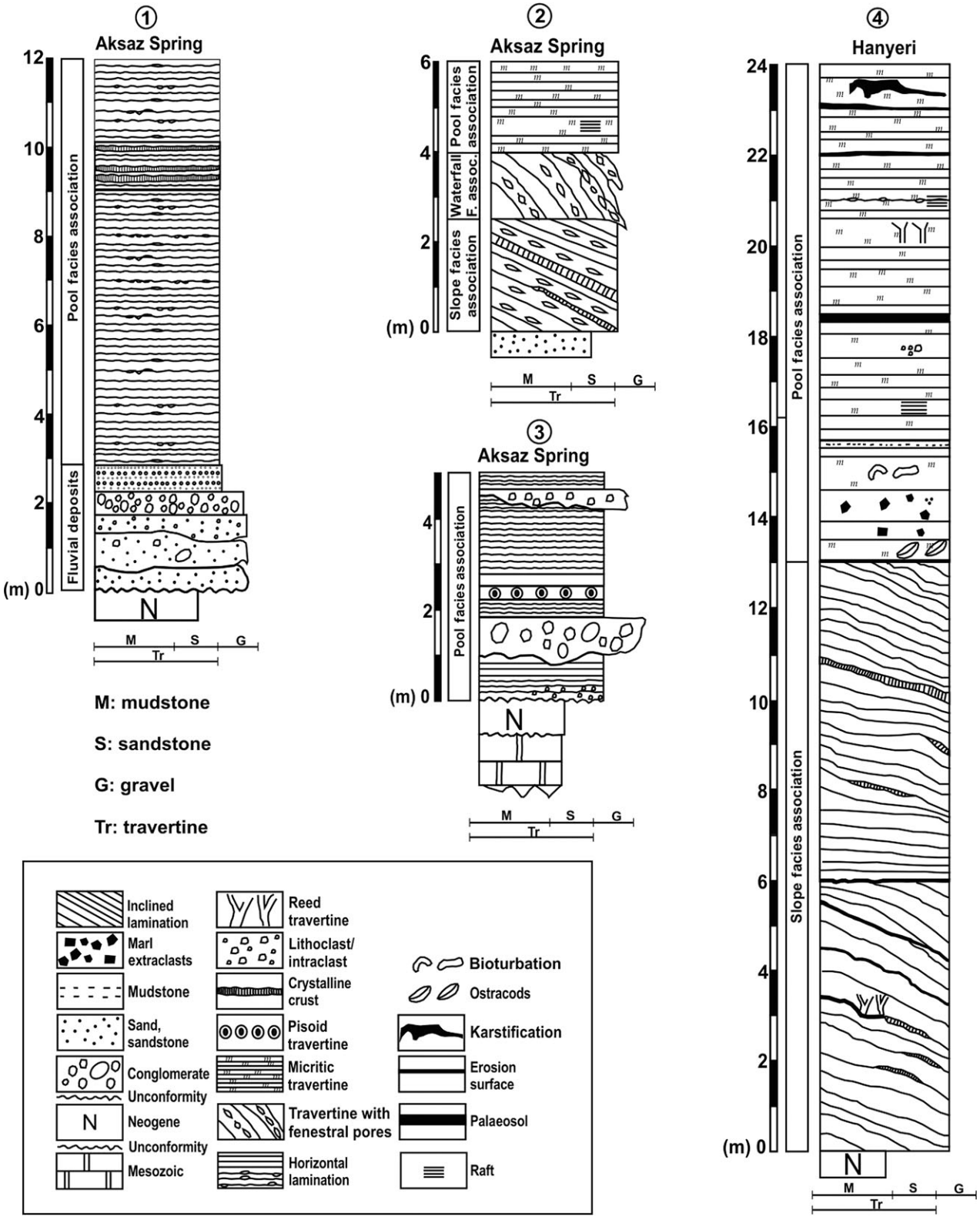

Fig. 2. Measured sections along the Aksaz Stream valley. The travertine successions are associated and alternated with fluvial detrital deposits that are formed mainly of conglomerates, sandstones and mudstones at the bottom (see the sections Aksaz Spring 1 and 3). The numbers encircled at the tops of the sections indicate their location in Fig. 1. On the linear scale at the bottom of each section N, Neogene; M, Mud; S, Sand; G, Gravel; Tr, Travertine.

elevations to lower elevations that are closer to the stream bed. The youngest generation of travertine close to the present stream bed is deposited around the Uyuz thermal spring and the bath ruins of the early Roman period (Fig. 1), located at *ca* 200 m upstream of the Aksaz thermal spring (Fig. 1D). A travertine sample collected close to these ruins gave a U-Th age of 1·848 ± 235 ka (Table 1), which confirms deposition during an early Roman period.

FACIES DESCRIPTION

At the field scale, facies descriptions of the travertines and associated sediments have previously been recognized from different geographical and geological settings (e.g. Chafetz & Folk, 1984; Guo & Riding, 1998; D'Argenio & Ferreri, 2004; Pentecost, 2005; Jones & Renaut, 2010; Renaut *et al.*, 2013). In the present study, facies corresponds to 'lithotype' as described in Guo & Riding (1998), and some extra descriptions are added to the previous list.

Crystalline crust

Description

Although crystalline crust is not a common facies in the study area, white and dense crusts of elongate calcite crystals up to 15 cm thick are preserved as subhorizontal-inclined lens-like layers (Fig. 3A), are sandwiched between darker micritic travertine beds and extend laterally up to 3 m. These layers are conformable with the underlying bedding plane. The feather calcite crystals in the crystalline crust layer are oriented normally to the depositional surface (Fig. 3B).

Interpretation

Crystalline crust layers precipitated on the inclined surfaces from fast flowing waters that are supersaturated with respect to $CaCO_3$ because of rapid CO_2 degassing (Jones *et al.*, 2005). Crystalline crust is a leading facies/lithotype of slope and waterfall sites (Chafetz & Folk, 1984; Guo & Riding, 1998; Özkul *et al.*, 2002; Jones & Renaut, 2008). In the case herein, crystalline calcite crusts occur as subhorizontal-inclined and lens-like layers in the slope facies association. These lens-like intercalations in old successions probably precipitate in close proximity to spring discharge areas. In all cases, elongate calcite crystals are arranged at right angles to the growth surface (Jones & Renaut, 2010). While younger crusts are commonly soft and easily crushed, as at Pamukkale (Kele *et al.*, 2011), older ones are typically hard and more resistant (Chafetz & Folk, 1984; Guo & Riding, 1998). Although crystal dendrites form in cold-water spring systems, they are commonly associated with hot springs (Turner & Jones, 2005). The morphology of the dendrite crystals has been attributed to a disequilibrium factor depending on various parameters, including the $CaCO_3$ saturation level (Jones & Renaut, 1995).

Pisoid travertine

Description

A lenticular layer of white pisoid grains (up to 1·5 cm in diameter) is observed at the lower part of the travertine sequence around the Aksaz Spring area (Fig. 1D). The irregular pisoid lens and pockets (up to 70 cm long and 5 cm thick) occur between yellow-coloured, laminated, thin, horizontally bedded travertine layers (Fig. 3C and D). The pisoid level laterally passes into the crystalline calcite layer. The grains are embedded in a sandy matrix, which is a milky brown colour but, in some cases, adjacent grains have point contacts (Fig. 3D). Although individual pisoids are usually spheroidal, mammilated grains are also evident (Fig. 3D). The mineralogical composition of the pisoids is calcite, based on the XRD measurements.

Interpretation

Pisoids (coated grains larger than 2 mm in diameter) are formed in terrace and cave pools, the cavities of self-built channels and spring orifices by agitated, drip and bubbling waters, respectively (Folk & Chafetz, 1983; Guo & Riding, 1998; Alçiçek *et al.*, 2005; Jones & Renaut, 2010). In the Aksaz case, the pisoids are formed at the spring orifice by the bubbling hot waters. Similar subrecent orifice pisoids composed of aragonite were formed from the bubbling thermal spring water, with a temperature of 57°C, saturated with respect to $CaCO_3$ at Çukurbağ, Pamukkale (Özkul *et al.*, 2013). Similar coated grains, formed of aragonite, up to 5 cm in size, have also been reported from the Tekkehamam geothermal field, close to Sarayköy town, south-west of the Denizli Basin (Richter & Besenecker, 1983). There, aragonitic ooids may have formed from the thermal waters (up to 99·7°C) that are of $Na–SO_4–HCO_3$ type (Şimşek, 2003), high supersaturation level (Sc: 0·6 to 0·7) with respect to $CaCO_3$ and rapid CO_2 degassing (Özkul *et al.*, 2013).

Fig. 3. (A) An image from the lens-shaped crystalline calcite layer with thickness of *ca* 15 cm preserved between two brown layers, Aksaz Spring area. The age of the sample is 42·9 ka (see Table 2). (B) SEM image of crystalline calcite displaying the dendritic growth in (A). Growth is to the right. (C) Pisoid lens between yellow-coloured, thin and horizontally bedded travertine layers, possibly formed in a spring orifice. (D) Close-up view of pisoid cluster in a fossil spring orifice, Aksaz Spring area. (E) Travertine lithoclasts and associated fluvial sandy matrix cemented by calcite. Travertine lithoclasts are probably reworked by fluvial processes.

Micritic travertine

Description

Dark (yellow to brown) and light-coloured micritic travertines occur as horizontally bedded and inclined layers and range from centimetres to several metres in thickness. However, in some cases, they show bed-parallel lens-like, millimetre-scale micropores and bundles of calcite rafts. The facies is composed mostly of micrite (i.e. fine crystalline to cryptocrystalline calcite) and alternated occasionally with lithoclast travertine, exposure surface and overlying palaeosol levels. The SEM images of some samples show ostracod, Chara, microbial filament and diatoms as embedded components in the micritic ground (Fig. 4A to D).

Interpretation

Micrite is one of the most widespread facies in tufa and travertine deposits (Sant'Anna *et al.*, 2004; Jones & Renaut, 2010). In the case of Aksaz, the facies is particularly widespread in the pool facies association that is horizontally bedded and aerially extensive. Although the origin of micrite is unclear, at least some parts may be microbially induced, as recorded in lake environments (Gierlowski-Kordesch, 2010). In the Itaboraí Basin, South-eastern Brazil, micritic travertines of Palaeocene age contain disseminated pyrite, minor amounts of detrital quartz, feldspar and scattered pebbles, which were attributed to the precipitation in small, shallow ponds under biotic mediation (Sant'Anna *et al.*, 2004).

Raft travertine

Description

The raft travertines occur as bundles of millimetric and delicate crystalline calcite layers (Fig. 5A and B). In some cases, they develop in horizontal laminae, several centimetres wide between adjacent reed stems in the micritic travertine facies, and alternate with reddish to brown millimetric intercalations. Under the SEM, the longitudinal calcite crystals that are growing downward have dentate tips (Fig. 5C). Alternating calcite layers of millimetre-scale vary in thickness (Fig. 5D). Near the Aksaz Spring, some raft formations are observed locally as deformed and sunken packages resting on one another, developed on the vertical surface of an older travertine block that has fallen down from the valley cliff side (Fig. 5E).

Interpretation

Raft travertine precipitates at the air–water interface in different settings, such as stagnant pools, around spring orifices and fissure spaces filled by hot waters (Chafetz *et al.*, 1991; Özkul *et al.*, 2002, 2013) and cave pools (Jones & Renaut, 2010). Rafts are thin and delicate crystalline sheets which are formed of calcite and/or aragonite where surface degassing of CO_2 causes an increase in saturation levels (Folk *et al.*, 1985; Chafetz *et al.*, 1991; Capezzuoli & Gandin, 2005); they are usually thickened due to subsequent encrustation (Guo & Riding, 1998; Jones & Renaut, 2010). Apparently ductile deformation of some raft packages at the Aksaz Spring area may have resulted from hot waters saturated with respect to calcite being occasionally accompanied by explosive rapid CO_2 degassing events under high pressure, as in Pamukkale (Uysal *et al.*, 2009). On the other hand, the wavy travertine laminae resembling rafts may have been precipitated on vertical or highly inclined surfaces from slowly flowing sheets of thermal waters (Fig. 5E). In the Aksaz Spring area, present-day equivalents of these wavy laminae are associated with microbial activity.

Reed travertine

Description

Reed facies is observed infrequently as moulds of aquatic plants in growth position, with stabilized root systems. It is associated with the facies of 'micrite travertine', 'travertine with fenestral pores' and calcite rafts. The reed clusters, which are branched and extended upwards, reach up to 80 cm long. Inner parts of the tubular reed moulds (up to 1 cm in diameter) coated in a brown colour are mostly empty, and cause high primary porosity. Dense reeds seem to obscure the image in highly inclined or vertically exposed surfaces of travertine sequences.

Interpretation

Reed facies is widespread in different depositional settings, such as mound, waterfall or cascade facies of travertine and tufa systems (Ford & Pedley, 1996; Guo & Riding, 1998; Arenas *et al.*, 2000; Arenas-Abad *et al.*, 2010; Jones & Renaut, 2010; Özkul *et al.*, 2013). It is very common in the mound and waterfall (or cascade) facies at the upper parts of the travertine-tufa sequence of the Ballık area near Kaklık in the north-east of the Denizli Basin, western Turkey

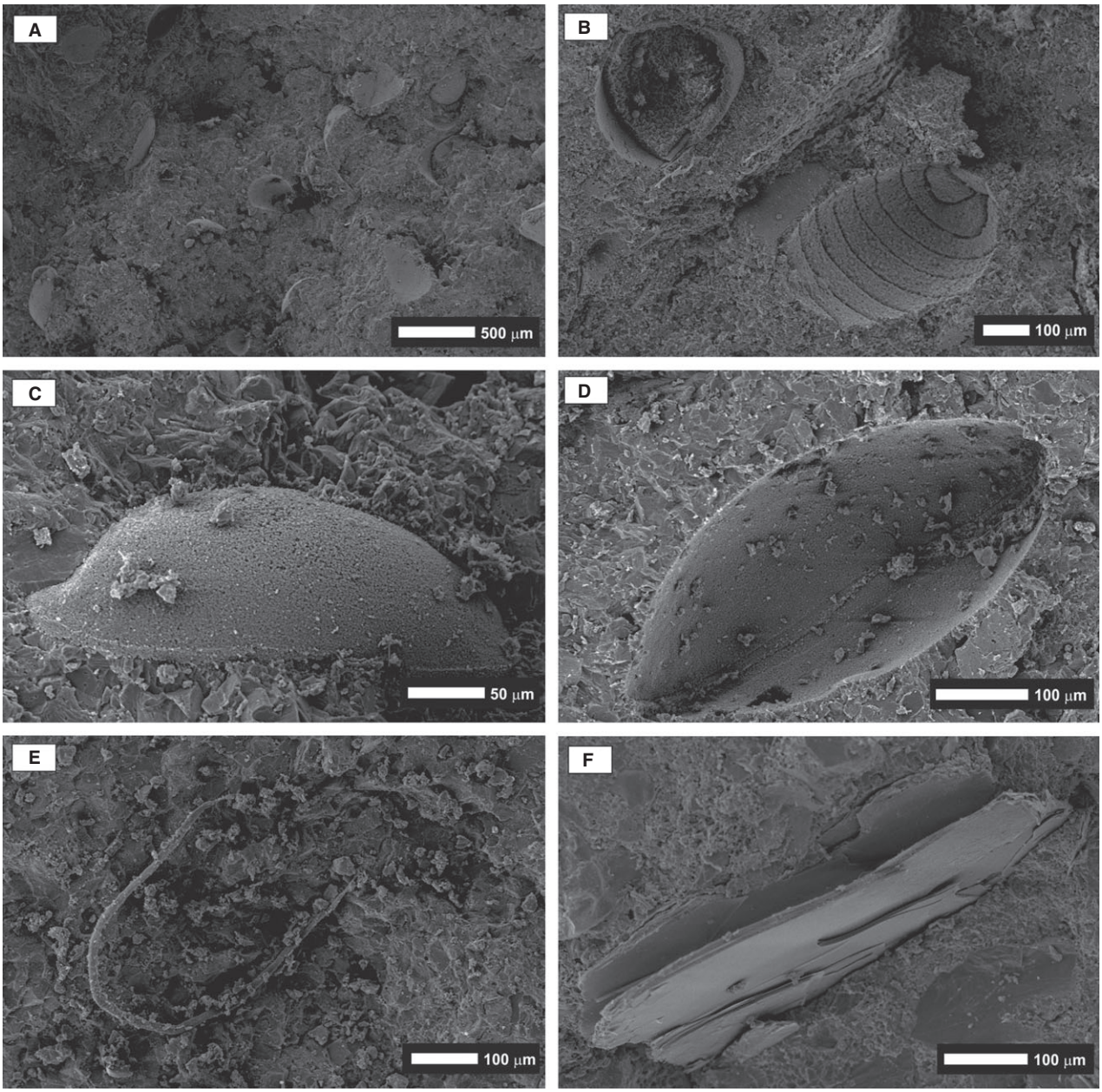

Fig. 4. Scanning electron microscope images of fossil components entombed in micritic travertine facies. Ostracod shells (A) and Chara mould in a micritic ground (B). (C) and (D) Outer and inner cast of ostracods. (E) Curved filamentous cyanobacteria and (F) Diatom frustule. Middle and upper parts of the Hanyeri section measured from the quarry near the village of Hanyeri (see Figs 1 and 2 for location and stratigraphic position, respectively).

(Özkul *et al.*, 2002, 2013; Van Noten *et al.*, 2013). In contrast, the facies rarely occurs in the slope and pool travertines of the Aksaz area.

Lithoclast travertine

Description

The lithoclast travertine is exposed mostly as pockets and interbeds, with thicknesses of up to 50 cm, within the horizontally bedded travertines and the lower part of the waterfall travertines (Fig. 2). The facies is composed of light-coloured, angular to sub-angular travertine clasts in varying sizes up to 20 cm diameter (Fig. 3E). The matrix is mostly sand of fluvial origin. In some cases, travertine clasts are observed as mixed with siliciclastic material at the bottom of waterfall travertine bodies.

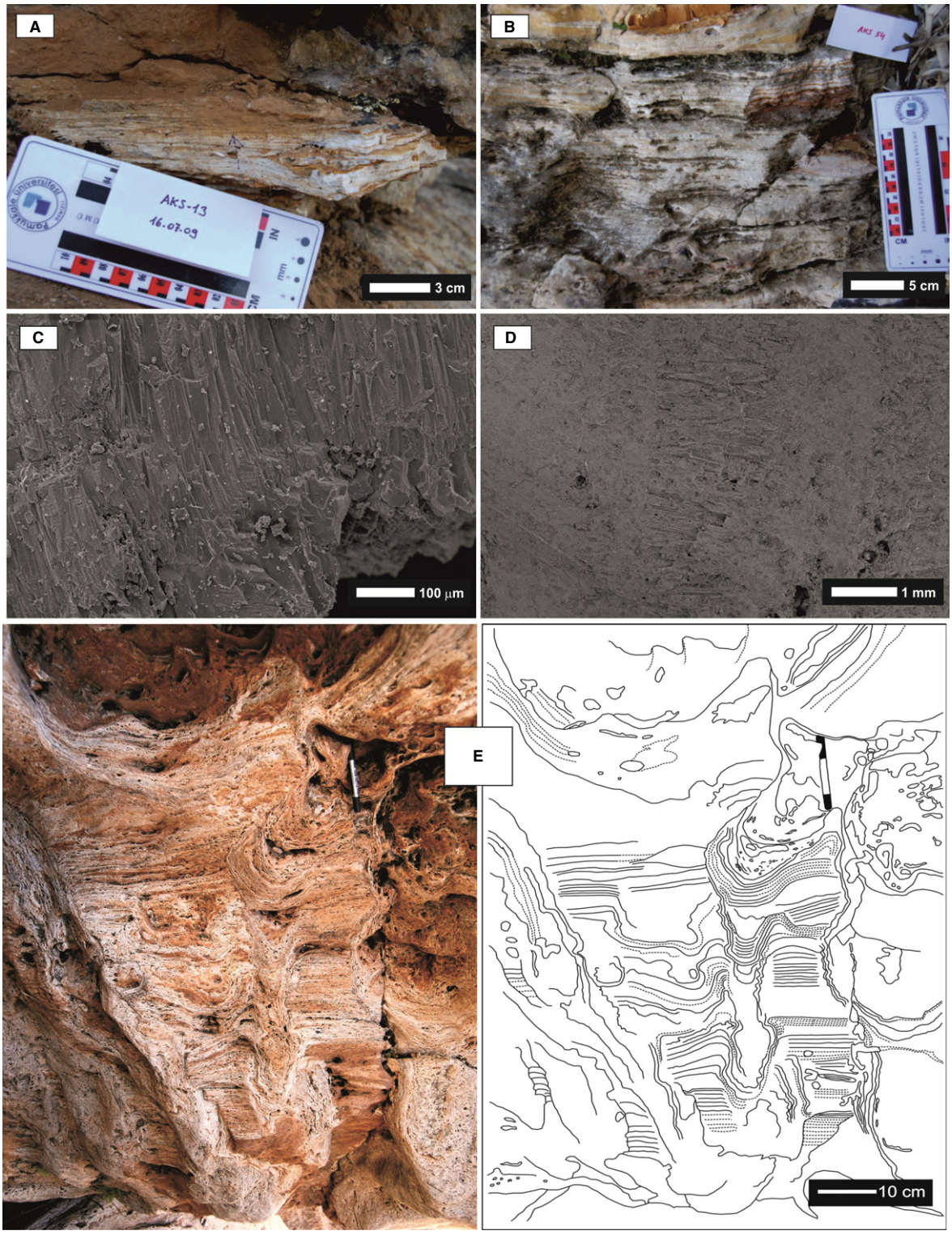

Fig. 5. Field and Scanning electron microscope (SEM) images of the raft and laminated travertines of the Aksaz Spring area. (A) Parallel-laminated raft bundles formed of calcite. (B) Thick raft bundles, up to 40 cm thick, note the white laminae that alternate with red ones. (C) SEM image of longitudinal calcite crystals with dentate tips, grown downwards. (D) SEM image of alternation of thin and thick calcite crystal layers at a millimetre scale. (E) Deformed and wavy laminae packages, accumulated on one another that display different generations from a palaeospring that has discharged, possibly through a collapsed older travertine block standing in the valley bottom nearby the Aksaz Spring.

Interpretation
Coeval erosion and breakage of spring carbonates (for example, travertine and tufa) in slope and waterfall settings produce lithoclasts, bioclasts and phytoclasts in large quantities. Erosion usually results from water flow and flooding after occasional heavy rains (Guo & Riding, 1998; Arenas-Abad *et al.*, 2010; Jones & Renaut, 2010). Lithoclastic material derived in this way is transported downslope and accumulates in depressions and ponds located in distal areas or around obstacles on the lower slope surface. Fluvial erosion is thought to be the most prominent process for the lithoclast production in the study area.

Travertine with fenestral pores

Description
This facies is formed of alternating porous and less porous layers, which are usually members of the waterfall and partly the slope facies association in the study area (Fig. 6A to D). In the Aksaz Spring area (Fig. 1D), the facies is underlain by 'conglomerate and sandstone facies' at the basal part of the waterfall facies association (Fig. 7). The pores are mostly lenticular to flattened in shape, a few millimetres to centimetres long and arranged crudely along the bedding planes (Fig. 6A and C). Rarely, they comprise closely associated reed tussocks in growth position.

Interpretation
This facies possibly results from seasonal or periodic desiccation of bacterial–algal mats on gentle to steep slope and waterfall depositional surfaces (Fig. 7). The pores in this facies resemble 'fenestral cavities' (Rainey & Jones, 2009) or birds-eye type pores developed in intertidal limestones (Chafetz & Folk, 1984). Microbial activity and associated slow sheet flow, responsible for porous layers, possibly was induced in the spring and summer seasons, while the succeeding dense layer precipitated during the winter season. Subsequent loss of microbial mats (for example, bacteria, cyanobacteria and diatoms) through decay has produced distinctive elongate biomoulds (Jones & Renaut, 2010).

Palaeosol

Description
Near the Aksaz Spring, brown-coloured, mud-rich palaeosol horizons, ranging from a few to 15 cm in thickness, with scarce fine pebbles, some of which are travertine lithoclasts, alternate with light-coloured crystalline calcite layers with sharp contacts (Fig. 6E). In the horizontally bedded travertines along the quarry faces near the Hanyeri village (Figs 1 and 2), the palaeosol layers along the erosion surfaces can be followed over a distance of a few tens of metres.

Interpretation
Erosion and soil formation are widespread in travertine sequences. Erosion surfaces and associated palaeosol occurrences form boundaries between succeeding travertine sequences. Variations in spring location and direction of water flow result in exposure of travertines to subaerial conditions and subsequent palaeosol formation that is encouraged mostly by desiccation and biological activities (Chafetz & Folk, 1984; Guo & Riding, 1998; Özkul *et al.*, 2002; Faccenna *et al.*, 2008). Erosion surfaces and overlying palaeosol layers in the Aksaz area are more common in the horizontally bedded travertines precipitated in extensive pool environments.

Conglomerate and sandstone

Description
Conglomerate and sandstone horizons are located at the base and the lower part of the travertine sequences, as in measured sections 1, 2 and 3 in the Aksaz Spring area (Fig. 2). These coarse to fine-grained siliciclastics are mostly polygenic and, to a lesser extent, monogenic in character. The polygenic conglomerates are poorly sorted, mainly clast-supported and are composed principally of quartzite, schist, sandstone and limestone clasts that usually are angular to subangular. On the other hand, the monogenic conglomerates are matrix-supported and carbonate-cemented and are formed mostly of marl or lacustrine limestone of Neogene age (Fig. 6F), situated in the middle and upper levels of the travertine sequences (metres 13 to 15 of the Hanyeri section in Fig. 2). The tabular or cross-bedded sandstones are loose and poorly lithified and include bee nests in some exposures; occasionally, they are laterally interfingered with travertine layers. Conglomerate and sandstones are derived primarily from the metamorphic and subsequent Neogene sedimentary bedrocks in the catchment area of the Aksaz Stream (Figs 1 and 2). In contrast, the monogenic conglomerate was derived locally only from adjacent Neogene beds and washed into the travertine depositional environments.

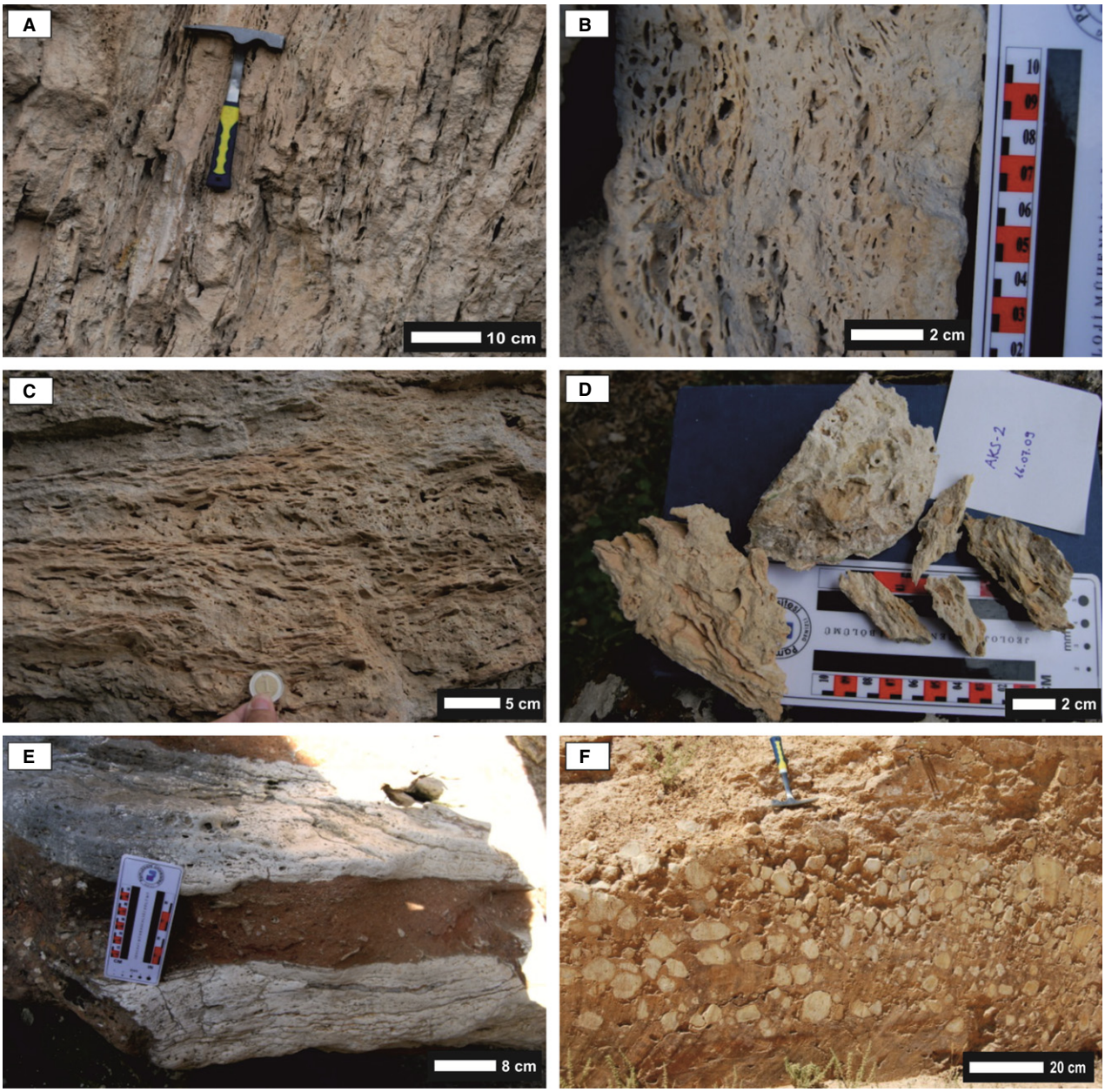

Fig. 6. Field and hand specimen images of the 'travertine with fenestral pores' facies, palaeosol and conglomerate. (A) Vertically to subvertically oriented 'travertine with fenestral pore' facies formed of alternating porous and less porous layers. (B) A close-up view of the porous and less porous layers in (A). (C) Horizontal porous layers developed locally. (D) A hand specimen containing fenestral pores, with brown-coloured inner surfaces, possibly originating from microbial activity (Sample AKS-2). (E) Brown palaeosol (in the middle) sandwiched by light crystalline calcite layers. (F) Monogenic conglomerate formed of marl clasts enclosed as an interbed in the horizontally bedded travertines of the pool facies association, drifted from the adjacent Neogene succession, metres 13 to 15 of the Hanyeri section quarry faces, (see Figs 1 and 2 for location and stratigraphic level, respectively).

Interpretation

Detrital deposits have previously been reported at the base of Quaternary fluvial tufa sequences from arid and semi-arid regions of Namibia (South Africa) and Spain, respectively. For instance, in arid conditions, fluvial channels are filled by reworked tufa and coarse detrital clasts, up to a boulder size of 3 m, which indicates local inputs from hill slopes (Viles *et al.*, 2007). In the semi-arid case of Spain, detrital deposits, exposed at the base of the outcrops, cover erosional surfaces accompanied by varying incision

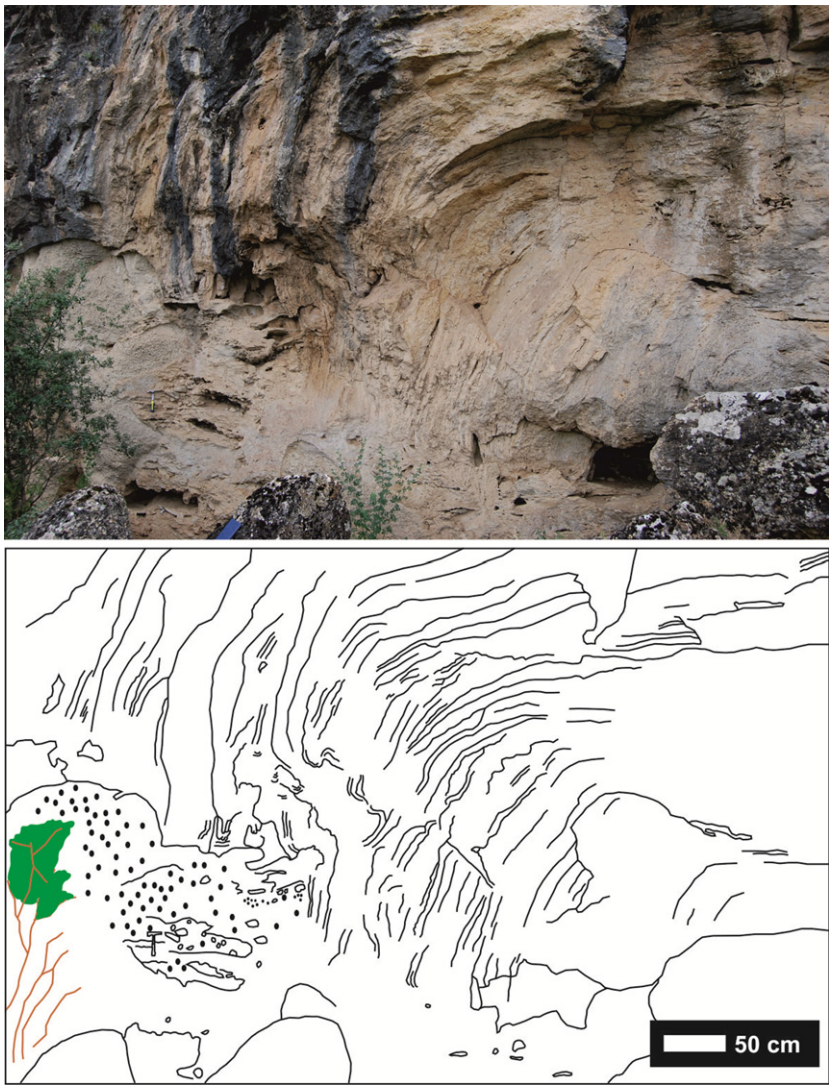

Fig. 7. Waterfall facies associations, dipping to the north-east, represented mostly by the facies 'travertine with fenestral pores', in which highly inclined porous and less porous layers are alternating (see Fig. 6A to C). The highly inclined or overhanging layers of the waterfall facies associations overlie poorly cemented basal sandstones of fluvial origin (dotted area in the drawing to the lower left). Location is between the Aksaz Spring area and Roman bath (see Fig. 1).

of the underlying bedrocks (Vázquez-Urbez *et al.*, 2012). In the study area, coeval detrital material (for example, conglomerate and sandstone), accumulated in lenticular and/or tabular bodies along the Aksaz Stream channel, arises during the early stages of travertine precipitation.

FACIES ASSOCIATIONS

In this study, facies associations are established by considering the various combinations of characteristic facies (cf. 'lithotype' of Guo & Riding, 1998), together with their depositional morphology and profile details. In this context, three associations are established: (i) waterfall facies association; (ii) slope facies association; and (iii) pool facies association.

Waterfall facies association

The waterfall facies association has been observed at two points between the Aksaz Spring and Roman bath (Fig. 1D). Downstream-facing deposits, with lobate, mound-like morphologies (Figs 7 and 8B), appear to be perched springline tufa (Pedley *et al.*, 2003; Özkul *et al.*, 2010) up to several metres thick. The most prominent facies of this association is 'travertine with fenestral pores' (Fig. 6A to D) that are formed by overhanging porous and less porous layers (Fig. 7), and subsidiary reed travertine. Waterfall overhang deposits consist predominantly of the crystalline crust travertine lithotype at Rapolano Terme, central Italy (Guo & Riding, 1998). In some cases, at Aksaz, the waterfall tufa develops directly on the detrital subordinates of sandstones and conglomerates of fluvial origin (Fig. 7). The association is

transitional or developed on the gently sloping travertine and overlain by horizontally bedded travertines of the pool facies association (Fig. 8B).

Waterfalls are common features of tufa and travertine systems (Pedley, 1990; Ford & Pedley, 1996; Guo & Riding, 1998; Martín-Algarra *et al.*, 2003; Anzalone *et al.*, 2007; Özkul *et al.*, 2010);

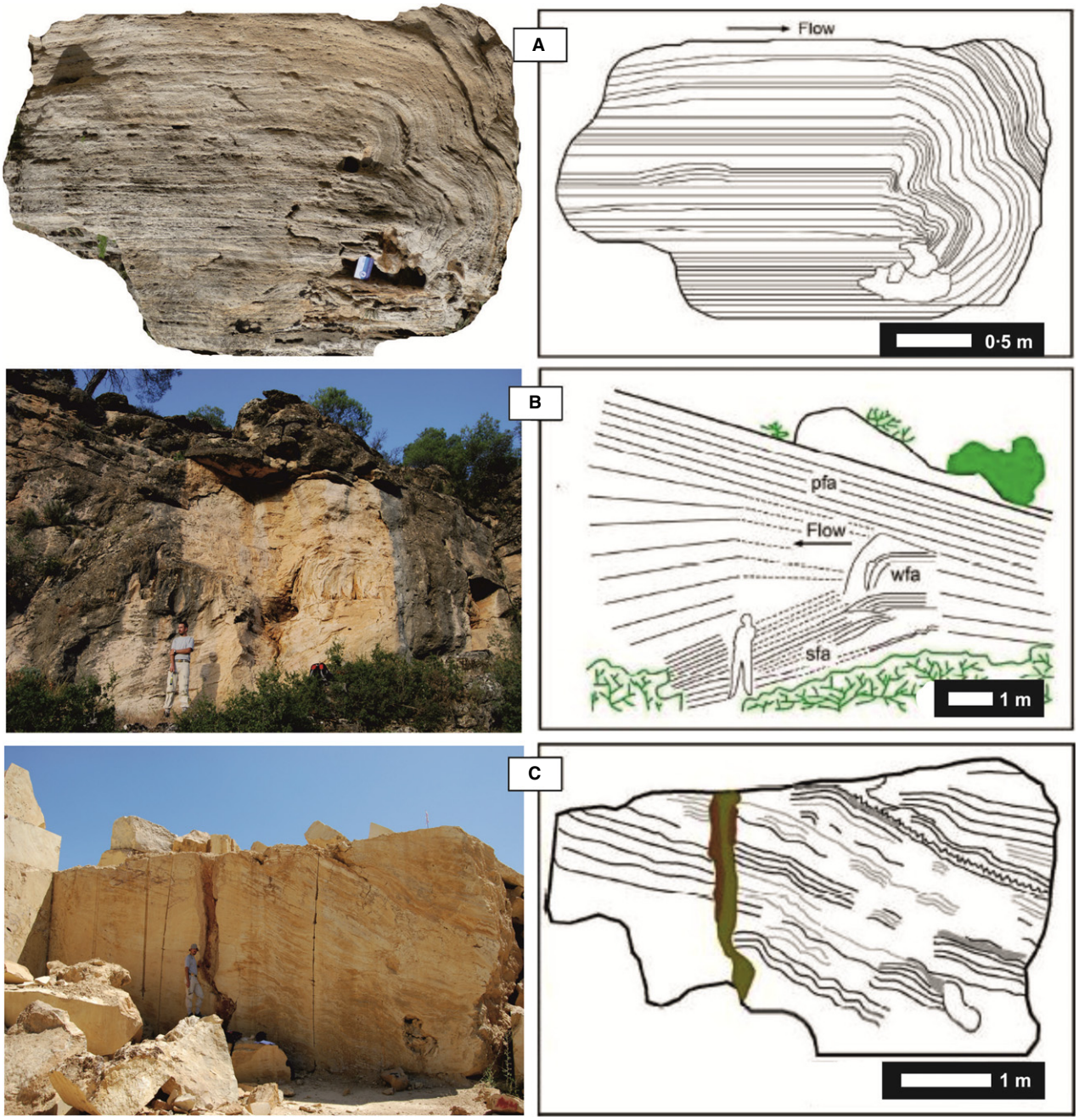

Fig. 8. Field images of the waterfall and slope facies associations in the Aksaz travertines. (A) Terraced slope travertines. The terrace pool is filled mostly by horizontally bedded micrite and the terrace wall is bounded by vertically laminated micrite. Flow direction is indicated by an arrow at the top. Location: Aksaz Spring area. (B) Smooth slope travertines (sfa) overlain by the waterfall facies associations (wfa), at the top, and horizontally bedded travertines of the pool facies association (pfa) cover all of the sequence, upstream of the Aksaz Spring area. (C) Smooth slope travertines composed of brown to yellow micritic travertine accompanied by white crystalline crust intercalations. An exposure surface is indicated by a sawtooth line at the top right, lower part of the Hanyeri section measured (see Fig. 2).

however, they are less common in thermal spring systems (Chafetz & Folk, 1984; Guo & Riding, 1998). In the study area, waterfall travertines developed downstream from thermal springs issuing from the moderate to high-angle slopes and stepped stream profile.

Slope facies association

The slope facies association commonly develops as a smooth slope with occasional terraced parts (Fig. 8A). The angles of smooth slope surfaces range from 10° to 40°. Around Hanyeri and the Aksaz Spring area (Fig. 1D), quarry face exposures of this facies association show that the deposits are up to 5 m thick and extend more than 7 m laterally (Fig. 8B and C). At Hanyeri, the upper part of the slope sequence is scoured by a 3·2 m wide and 1·6 m deep channel that is subsequently filled. In most cases, although crystalline crust is a dominant facies (or lithotype) of the slope depositional system (Guo & Riding, 1998; Özkul *et al.*, 2002; Jones & Renaut, 2010), in the present case, it is not common in the quarry faces (for example, lower part of the Hanyeri section in Fig. 2) and natural cliff exposures. Therefore, the association consists mainly of facies 'travertine with fenestral pores' and micritic travertine, which is wavy bedded–laminated along with subsidiary crystalline crust layers and rare reed moulds. The slope facies association is laterally and vertically transitional with waterfall and pool associations (Fig. 8B). The slope facies association occurs where the springs emerge on hillslopes or topographic breaks along the stream valley (Fig. 9).

Pool facies association

The pool facies association, horizontally bedded and laterally extensive (up to several tens of metres based on exposure conditions), is formed mainly of micritic travertine (Figs 2, 10A and 10C). The thickness of the succession apparently varies between 2 m and 12 m. Light and dark layers alternate in some quarry faces (Fig. 10B and C; cf. 'Shrub Flat Facies' and 'Marsh-Pool Facies' of Guo & Riding, 1998). Erosion surfaces, palaeosol layers and accompanying karstification are common features, particularly in the uppermost parts of the successions (for example, the Hanyeri section, Fig. 2). The erosion surfaces and associated palaeosol horizons constitute sequence boundaries between the successive travertine packages, as in the Hanyeri section (Figs 2 and 10A). In addition, interlayers of lithoclast travertine (Figs 3E and 10B), claystone and mudstone are widespread intercalations (Fig. 10B and C). The facies association develops in the extended parts of the valley floor (Fig. 9). These parts of the valley floor are relatively extensive shallow flats or depressions, which are fed predominantly by thermal springs (Chafetz & Folk, 1984; Guo & Riding, 1998).

Previously, this facies association in Italy has been described as 'shallow lake-fill deposits' at Bagni di Tivoli east of Rome, (Chafetz & Folk, 1984) and 'shrub flat facies' and 'marsh-pool facies' at Rapolano Terme (Guo & Riding, 1998). These environments correspond to the pooled areas which are similar to shallow lakes and floodplains in fluvial tufa systems (Vázquez-Urbez *et al.*, 2012).

TRAVERTINE GEOCHEMISTRY

Major and trace elements

Elemental abundances of 23 travertine samples are given in Table 3. The highest concentrations are those of Ca and Mg. Sample AKS-9, which has the lowest Ca and Sr values, has the highest Si, Fe and Mn values (Table 3), which are attributed to a significant detrital content. The common origin of Fe and Mn is also shown by samples consisting of crystalline calcite (sample AKS-18) where the detrital contamination is negligible.

The Sr content ranges from 319 to 3432 ppm with a mean value of 1131 ppm in the samples that are formed of calcite. The highest Sr content, up to 3432 ppm, is measured from a crystalline calcite travertine sample (AKS-33, Table 3) that is taken from the younger generation nearby the historical Roman bath (Fig. 1D). Uranium contents of the travertine samples range from 0·2 to 6·3 ppm, while the Th contents are between 0·2 and 1·6 ppm (Table 3).

Stable isotope composition of the Aksaz travertines

The $\delta^{13}C$ and $\delta^{18}O$ values range between +4·3‰ and +6·3‰ and between −12·6‰ and −7·2‰ (VPDB), respectively (Table 4 and Fig. 11). In addition, two additional subsamples were taken for stable isotope analyses from a recent

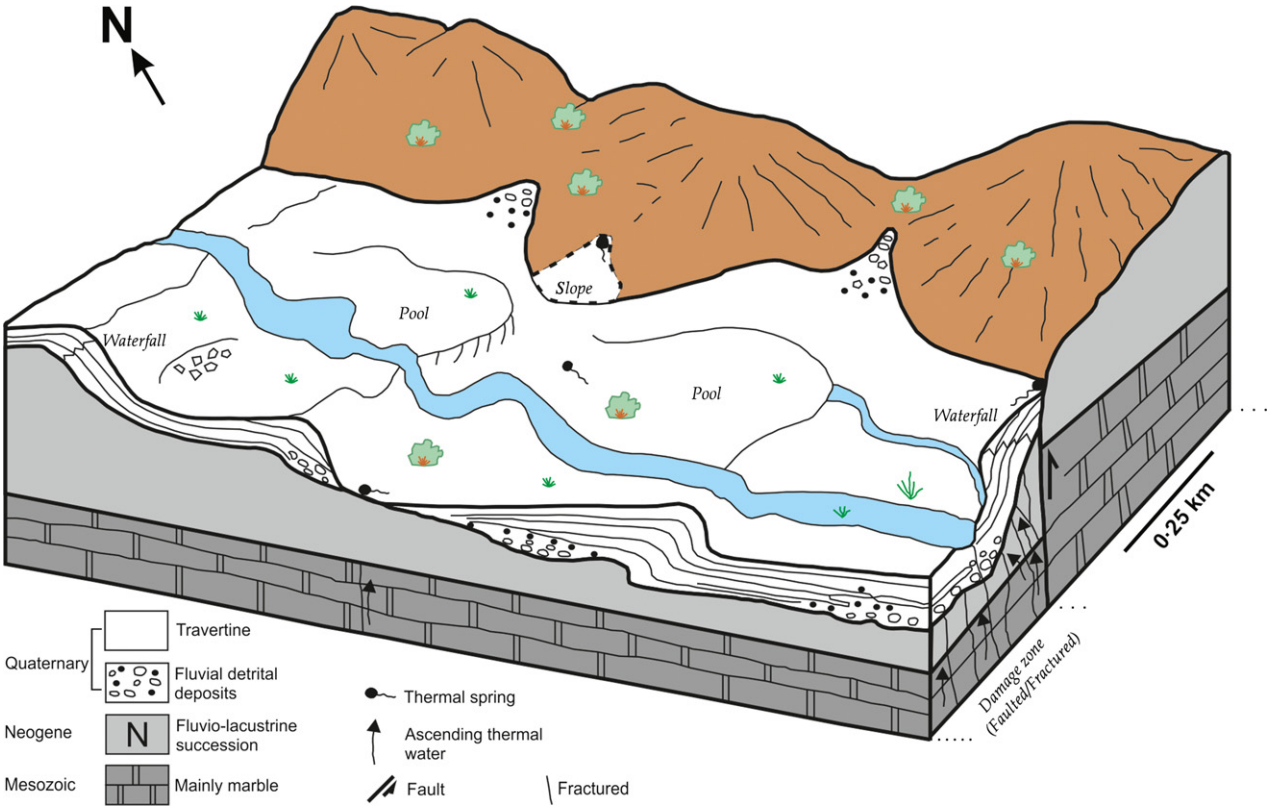

Fig. 9. Interpretive depositional model for fluvial travertines along the ephemeral Aksaz Stream valley. The NW-trending stream valley was established in the damage zone of a tectonic line (for example, fault and/or fracture). Springs emerged on a hilly topography precipitate waterfall and slope facies associations, whereas horizontally bedded travertines of the pool facies association accumulate in extensive pools/depressions restricted to areas of the stream valley fed by thermal springs.

travertine sample deposited directly at the orifice of a thermal seep 50 m downstream of the Aksaz Spring. The surface of the sample shows higher values ($\delta^{13}C$ +6‰; $\delta^{18}O$ −11·0‰) than the inner part ($\delta^{13}C$ +5·7‰; $\delta^{18}O$ −11·5‰; Table 4; Fig. 11).

Palaeotemperature calculations

Palaeotemperature calculations are based on the $\delta^{18}O_{calcite}$ values and the $\delta^{18}O_{water}$ but, in the case of fossil travertine deposits, the $\delta^{18}O_{water}$ value is not known and must therefore be inferred (Andrews *et al.*, 2000). The deposition temperature of travertines is generally calculated by the equations of Friedman & O'Neil (1977) (Eq. 1) or Kim & O'Neil (1997) (Eq. 2), assuming equilibrium oxygen isotope fractionation between travertine and water during carbonate precipitation:

$$10^3 \ln\alpha_{c-w} = (2{\cdot}78\times10^6)/T^2 - 2{\cdot}89 \qquad (1)$$

$$10^3 \ln\alpha_{c-w} = (18{\cdot}03\times10^3)/T^2 - 32{\cdot}42 \qquad (2)$$

where: $\alpha_{c-w} = (\delta^{18}O_{calcite} + 1000)/(\delta^{18}O_{water} + 1000)$ and $10^3 \ln \alpha_{c-w} \approx \delta^{18}O_{calcite} - \delta^{18}O_{water}$.

However, this calculation is further complicated by the fact that isotopic equilibrium is rarely maintained under natural conditions for actively depositing carbonates (e.g. Coplen, 2007; Kele *et al.*, 2008, 2011). At Aksaz Spring, it was possible to test the reliability of the above equilibrium equations (Eq. 1 and Eq. 2) for palaeotemperature calculations because the deposits are recent and the associated parent waters that allow comparison of the measured and calculated temperature of deposition. Using the average $\delta^{18}O_{calcite}$ value of the recently deposited vent travertine sample (19·4‰, VSMOW) and the $\delta^{18}O$ of the spring water (−9·2‰, VSMOW) the measured $1000\ln \alpha_{c-w}$ is 28·59‰, which is higher than those calculated using Eq. 1 of Friedman & O'Neil (1977) (26·26‰) and

Fig. 10. Field images of the pool facies association. (A) Pool facies association formed of horizontally bedded and laterally extensive micritic travertines with erosion surfaces (es), karstification and lithoclast layers at the uppermost quarry face, Hanyeri (cf. upper half of the Hanyeri section in Fig. 2). (B) Alternating light and dark horizontal travertine layers with lithoclast layer (lt) in the middle. The light and dark layers correspond to the 'Shrub Flat Facies' and 'Marsh-Pool Facies' of Guo & Riding (1998), respectively. (C) The two travertine packages are separated by a green mudstone layer (indicated by arrows).

those calculated by Eq. 2 of Kim & O'Neil (1997) (26·18‰). These calculations clearly demonstrate that precipitation of the calcite currently is not in isotopic equilibrium with the spring waters of the Aksaz Spring; thus, the use of the Friedman & O'Neil (1977) and Kim & O'Neil (1997) equilibrium equations produces underestimations of the actual temperature. Kele *et al.* (2008, 2011) demonstrated that $1000\ln\alpha_{c\text{-}w}$ values of vent travertines show a quasi constant positive shift relative to the equilibrium and emphasized that this deviation can cause the calculated temperature to be 8 to 9°C lower than the true temperature. Thus, palaeotemperature values calculated with one of the above-mentioned equations must be increased by 8 to 9°C

Table 3. Element composition of the Aksaz travertine samples.

Sample No.	Ca (ppm)	Si (ppm)	Fe (ppm)	Mg (ppm)	Mn (ppm)	Sr (ppm)	U (ppm)	Th (ppm)
AKS-3B	393500	1447	350	3558	310	1077	0·8	<0·2
AKS-8A	391857	1446	1960	1930	232	607	3·1	0·2
AKS-8B	400571	560	770	1688	155	922	1·0	<0·2
AKS-9	346071	34440	7035	3377	542	655	0·7	1·4
AKS-11	386929	3733	2555	3558	232	1067	0·4	1·1
AKS-13	373571	10313	4025	4161	310	1285	0·7	0·4
AKS-14	394214	1400	805	2110	155	406	3·3	<0·2
AKS-16	390071	1493	770	3136	nd	1027	1·0	<0·2
AKS-17	389214	2987	315	3980	nd	1425	0·9	<0·2
AKS-18	389571	980	nd	6150	nd	2379	1·5	<0·2
AKS-22	395142	4667	665	2171	78	978	0·5	<0·2
AKS-24	371214	13393	1470	4462	78	848	0·4	1·6
AKS-27	390286	2427	2940	5849	232	1223	6·3	<0·2
AKS-28	383214	1307	6230	4281	611	946	0·9	<0·2
AKS-31	390071	2193	2695	1507	465	535	2·4	<0·2
AKS-33	390429	4013	1190	4341	78	3432	1·0	0·6
AKS-34	380357	7887	980	6392	78	2051	0·8	0·9
AKS-36	395357	140	1540	3015	78	1042	1·1	<0·2
AKS-37	392214	2007	2310	1387	154	319	0·2	<0·2
AKS-41	390071	1260	3395	844	232	530	0·5	<0·2
AKS-43	376286	6440	7735	1085	387	412	1·5	0·3
AKS-48	396285	4667	245	3136	233	1722	0·7	<0·2
AKS-54	394071	840	1890	2050	154	1129	0·5	<0·2

to obtain the most reliable palaeotemperature data.

Recently measured spring water $\delta^{18}O$ composition (−9·2‰) and the $\delta^{18}O$ values of the fossil travertine samples of Table 4 were used to calculate palaeotemperature values of the Aksaz Spring. Thus, it was assumed that the oxygen isotope composition of the palaeosprings was similar to that of the current springs. During the calculations, the calculated $1000\ln\alpha_{c\text{-}w}$ values were corrected with the recently observed deviation in the $\Delta_{calcite\text{-}water}$ values. Table 5 shows the results of these palaeotemperature calculations. Calculations based on the equilibrium equations (Eq. 1 and Eq. 2) of Friedman & O'Neil (1977) and Kim & O'Neil (1997) provided ambiguous temperature values (between 6 to 31°C and 4 to 30°C, respectively), while the correction suggested by Kele *et al.* (2011) resulted in higher and more realistic temperatures (14 to 39°C and 12 to 38°C, respectively). If Eqs 1 and 2 are corrected with the recently observed deviation in the $\Delta_{calcite\text{-}water}$ values at Aksaz Spring, then the calculated temperatures are even higher than those determined by applying the corrections of Kele *et al.* (2011) and vary between 16 to 44°C and 14 to 42°C, respectively. By comparing the current temperature of the Aksaz Spring (T = 35·8°C) with the calculated values for the palaeosprings, it can be concluded that the temperature of the palaeosprings was slightly higher than the present-day temperature for the springs, but occasionally the temperature was significantly lower, which could have been caused by mixing with the water of the nearby Aksaz Stream.

DISCUSSION

Previously, at large scale, different depositional models have been proposed for tufa and travertine precipitating spring systems (Chafetz & Folk, 1984; Altunel & Hancock, 1993; Ford & Pedley, 1996; Guo & Riding, 1998; Martín-Algarra *et al.*, 2003; Anzalone *et al.*, 2007; Pedley, 2009). No single classification scheme covers the full gamut of spring deposits. It has been suggested that cascade/waterfall, barrage (lacustrine), perched, paludal, fluvial, fissure and mound models can all be used both for tufa and travertine deposits (Jones & Renaut, 2010) because these schemes focus on the setting and general appearance and morphology of the deposits rather than water temperatures, facies, biota or mineralogy.

Spring carbonates in a fluvial setting

A fluvial setting is one of the leading models proposed for tufa deposits (Ford & Pedley, 1996;

Table 4. Stable carbon and oxygen isotope composition of the Aksaz travertines.

Sample No.	$\delta^{13}C$ (VPDB)	$\delta^{18}O$ (VPDB)	$\delta^{18}O$ (VSMOW)
AKS-1	5·7	−10·8	19·8
AKS-2	4·9	−12·0	18·5
AKS-3A	5·6	−12·0	18·6
AKS-3B	5·8	−11·8	18·7
AKS-4	6·0	−11·9	18·6
AKS-5	5·9	−11·9	18·7
AKS-6	5·1	−11·7	18·8
AKS-7	5·2	−12·1	18·4
AKS-8A	5·0	−11·8	18·8
AKS-8B	5·2	−12·6	17·9
AKS-9	4·3	−10·5	20·1
AKS-11	5·3	−10·0	20·6
AKS-13	5·2	−10·2	20·4
AKS-14B	5·3	−11·8	18·8
AKS-16	5·5	−10·6	19·9
AKS-19	5·6	−10·5	20·1
AKS-21	5·0	−7·2	23·5
AKS-22	5·6	−10·7	19·9
AKS-23	6·3	−8·8	21·8
AKS-24	4·9	−11·1	19·4
AKS-26	5·4	−11·9	18·6
AKS-29	5·1	−12·4	18·1
AKS-30	4·4	−12·3	18·2
AKS-32	5·5	−11·6	19·0
AKS-34	5·0	−11·3	19·3
AKS-35*	6·0	−11·0	19·5
AKS-36*	5·7	−11·5	19·0
Min.	4·3	−12·6	17·9
Max.	6·3	−7·2	23·5
Mean	5·35	−11·18	19·37

AKS–35* and AKS–36* are recent samples taken from a thermal seepage 50 m downstream of the Aksaz spring adjacent to stream water. The seepage is 1 m above with respect to the current stream water. VPDB, Vienna Pee Dee Belemnite; VSMOW, Vienna Standard Mean Ocean Water.

Arenas *et al.*, 2000; Pedley *et al.*, 2003; Pedley, 2009; Arenas-Abad *et al.*, 2010). However, the fluvial model was not suggested for travertine deposits prior to the present study. In the fluvial model, tufa-precipitating waters with shallow circulation are supplied by the springs, situated in the karstic valley.

Travertine occurrences in the south of Uşak province, western Turkey, have been precipitated by the thermal springs, with temperatures of *ca* 32 to 38°C, and are restricted mostly to the stream valleys trending north-east and north-west (Fig. 1C and D) that are established along tectonic lines. Some of the occurrences mentioned above, located along the Aksaz Stream valley (Fig. 1C), are elaborated on as a new case of travertine developed in a fluvial context, taking into account their depositional and geochemical characteristics.

Travertine deposits of the Aksaz Stream valley are composed mainly of waterfall/cascade, slope and pool facies associations, which were previously described only from different settings, such as mound and slope systems (Chafetz & Folk, 1984; Altunel & Hancock, 1993; Guo & Riding, 1998; Fouke *et al.*, 2000; Kele *et al.*, 2008, 2011). However, these facies associations also display lateral and vertical transitions in semi-continuous outcrops along the Aksaz Stream valley.

The waterwall and slope facies associations are the product of hot springs located on the hilly topography (Guo & Riding, 1998) or topographical breaks in the longitudinal profile of the fluvial tufa system (Vázquez-Urbez *et al.*, 2012), whereas the pool facies association precipitates in shallow and extensive pools where the valley bottom extends and the thermal spring waters are dammed locally (Chafetz & Folk, 1984; Guo & Riding, 1998; Özkul *et al.*, 2013). This kind of environment corresponds to the low-gradient area offered in tufa systems (Arenas-Abad *et al.*, 2010). In hot spring systems, the travertine sequence was precipitated in large ponds or lakes, swamp areas very likely to be fed by thermal springs, as in Süttő (Hungary), where the ponds and lakes are found at different altitudes and connected to each other with slope deposits and terraces (Sierralta *et al.*, 2010).

Temporal and spatial variations in spring location

Spring location is very important in the development of travertine facies (Guo & Riding, 1998; Pentecost, 2005; Jones & Renaut, 2010). Where springs emerge in hilly topography, waterfall and slope (or mound) travertines are precipitated, as in Pamukkale-Turkey (Altunel & Hancock, 1993; Şimşek *et al.*, 2000; Özkul *et al.*, 2002; Kele *et al.*, 2011) and Angel Terrace, USA (Fouke *et al.*, 2000; Fouke, 2011). On the other hand, horizontally bedded travertines accumulate from thermal spring waters that discharge into laterally extensive pools/depressions, such as those in Tivoli, 25 km east of Rome (Chafetz & Folk, 1984; Faccenna *et al.*, 2008), Rapolano Terme, Italy (Guo & Riding, 1998) and Ballık, Denizli, Turkey (Özkul *et al.*, 2002, 2013). In the study area, the present thermal springs emerge along the length of the Aksaz Stream valley and

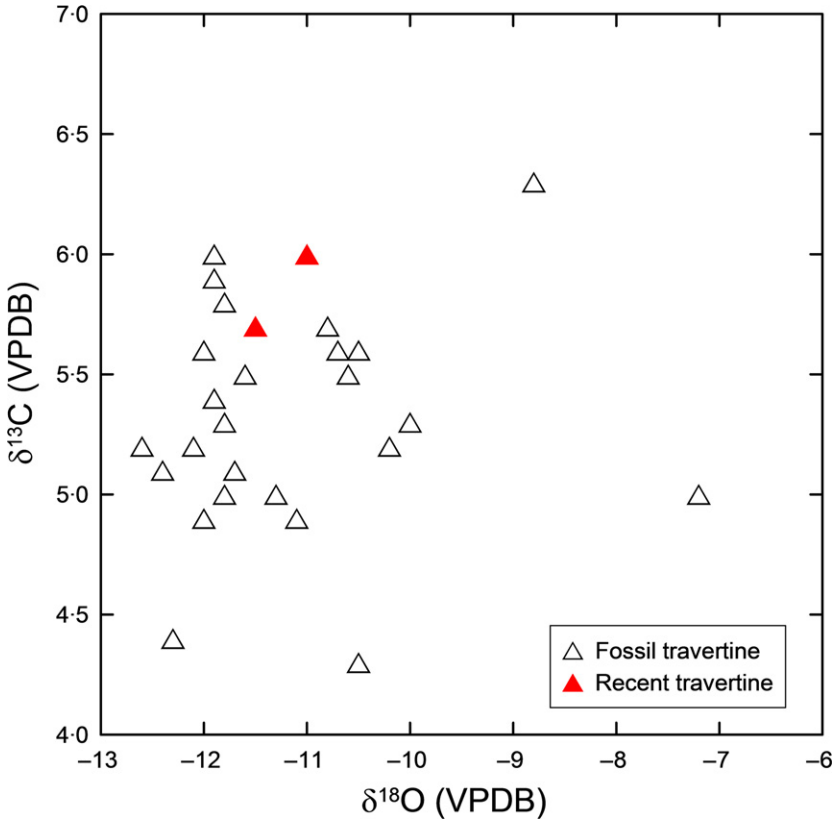

Fig 11. Stable carbon and oxygen isotopic compositions of the Aksaz travertine deposits.

according to the observations herein the travertine precipitation could have been restricted to a narrow zone (up to 2 km wide) in the past as well (Fig. 1C).

Precise locations of the palaeosprings are not clear in the Aksaz travertine field. However, it is possible to infer their locations from facies distribution and the vertical and lateral relations between them. Orifice pisoids and lenticular crystalline calcite crusts, which are sandwiched by distal precipitates (i.e. brown to yellow travertine beds), are possibly close to the spring locations. This relation indirectly implies that the hot springs have shifted over time. In addition, younger generations of the travertine deposits (for example, around the Roman bath thermal spring and Uyuz thermal spring (Fig. 1D) are closer to the present stream floor. Some of the subsequently emerging palaeosprings are discharged from the discontinuities (for example, bedding planes and fractures) within the older travertine blocks that collapsed onto the stream floor from the steep and unstable adjacent cliffs.

Most of the current thermal springs are located at the bottom of the present stream valley (Fig. 1). Consequently, either it is not possible or very difficult for the springs to precipitate travertine, although they are supersaturated with respect to calcite (saturation levels: 0·16 to 0·35). In the dry seasons, even if travertine precipitation occurred, it would be removed in the following wet seasons. Indeed, during the study period, significant travertine deposition was not observed; however, very limited deposition is recorded from thermal seepages up to *ca* 1 m above the stream floor. In the tropics of northern Australia, Carthew *et al.* (2006) observed that wet season floods remove the surface rafts and also flush out any sunken calcite rafts and mud accumulated during the dry season on the channel base. At Aksaz, thermal spring waters precipitated travertine most readily in places that were not influenced by the stream waters. In contrast, precipitation ceased and/or was washed out in the stream-influenced areas.

During the study period, several U-Th age data from the Aksaz travertines were obtained ranging from 153·11 ± 10 to 1·85 ± 0·24 ka (Table 1). The U-Th ages of 153 ka, 147 ka, 43 ka and 1·85 ka, which correspond to MIS 6, MIS 3 and MIS 1, respectively, mean that the travertines precipitating hot springs were active both in interglacial periods (for example, MIS 3 and MIS 1) and glacial periods (for example, MIS 6). This situation has also been confirmed

Table 5. Calculations of the temperature of deposition of the Aksaz travertines. For the calculations, the equilibrium equations of Friedman & O'Neil (1977) and Kim & O'Neil (1997) were used and were modified based on Kele *et al.* (2011).

Sample	$\delta^{18}O_{trav.}$ (SMOW)	$\delta^{18}O_{water}$ (SMOW)	Calc.[1] T(°C)	Calc.[2] T(°C)	Calc.[3] T(°C)	Calc.[4] T(°C)	Calc.[5] T(°C)	Calc.[6] T(°C)
1	19·8	−9·2	22	21	30	29	34	32
2	18·5	−9·2	28	27	36	35	40	39
3A	18·6	−9·2	28	26	36	34	40	38
3B	18·7	−9·2	27	26	35	34	39	38
4	18·6	−9·2	28	26	36	34	40	38
5	18·7	−9·2	27	26	35	34	39	38
6	18·8	−9·2	27	25	35	33	39	37
7	18·4	−9·2	29	27	37	35	41	40
8A	18·8	−9·2	27	25	35	33	39	37
8B	17·9	−9·2	31	30	39	38	44	42
9	20·1	−9·2	21	19	29	27	32	31
11	20·6	−9·2	18	17	26	25	29	28
13	20·4	−9·2	19	18	27	26	30	29
14B	18·8	−9·2	27	25	35	33	39	37
16	19·9	−9·2	22	20	30	28	33	32
19	20·1	−9·2	21	19	29	27	32	31
21	23·5	−9·2	6	4	14	12	16	14
22	19·9	−9·2	22	20	30	28	33	32
23	21·8	−9·2	13	11	21	19	24	22
24	19·4	−9·2	24	22	32	30	36	34
26	18·6	−9·2	28	26	36	34	40	38
29	18·1	−9·2	30	29	38	37	43	41
30	18·2	−9·2	30	28	38	36	42	41
32	19·0	−9·2	26	24	34	32	38	36
34	19·3	−9·2	24	23	32	31	36	35

Calc.[1] Based on Friedman & O'Neil (1977). Calc.[2] Based on Kim & O'Neil (1997). Calc.[3] Using the equation of Friedman & O'Neil (1977), modified based on Kele *et al.* (2011). Calc.[4] Using the equation of Kim & O'Neil (1997), modified based on Kele *et al.* (2011). Calc.[5] Using the equation of Friedman & O'Neil (1977), with $1000\ln\alpha_{c-w}$ correction. Calc.[6] Using the equation of Kim & O'Neil (1997), with $1000\ln\alpha_{c-w}$ correction.

in the travertine deposits of Denizli Basin (Özkul *et al.*, 2013).

Assessment of elemental and stable isotopic data

The highest Sr concentration measured in the Aksaz travertines is 3432 ppm (Table 3) indicating that the crystalline calcite travertine deposited around the Aksaz Spring area is closer to the palaeosprings than the adjacent beds. Recent crystalline crust calcite from the slope surfaces at Pamukkale has similarly high Sr values, up to 3028 ppm (Kele *et al.*, 2011, table 6).

Uranium contents of the Aksaz travertines range from 0·2 to 6·3 ppm, with a mean value of 1·3 ppm. However, the high U value of 6·3 ppm is obtained from the reed facies (sample AKS-27, Table 3). The U values mentioned above at Aksaz are similar to those of Pamukkale with a range of <0·1 to 9·6 ppm (mean: 0·9 ppm). On the other hand, elevated concentrations of a number of trace elements including Mn, Fe, Sr and U have been measured from the tufa deposits in the middle Miocene Barstow Formation, California, USA, that were possibly microbially mediated (Cole *et al.*, 2004). The U concentration of the Barstow tufa exceeds 500 ppm.

The $\delta^{13}C$ values of the Aksaz travertine range between +4·3‰ and +6·3‰ (VPDB) with an average of +5·4‰, while the $\delta^{18}O$ values are between −12·6‰ and −7·2‰ (VPDB) (Table 4, Fig. 11). High $\delta^{13}C$ values imply that the parent water was charged with CO_2 of deep origin. High $\delta^{13}C$ values for the Aksaz travertines imply that the parent water was charged with heavy CO_2 of deep origin. This heavy CO_2 in the study area could have been produced through decarbonation of carbonate bedrocks (i.e. Palaeozoic marbles and Miocene lacustrine limestones). Similar processes have been suggested for the more positive $\delta^{13}C$ values of travertine deposits

at Pamukkale (Kele *et al.*, 2011) and those along the northern boundary of the Denizli Basin; (Özkul *et al.*, 2013).

The temperatures and stable isotope composition of the recent travertines collected in or close to the spring vents at Aksaz and Pamukkale show similar values (Kele *et al.*, 2011; Fig. 12). The water temperature of the Aksaz Spring is *ca* 32 to 38°C, while the springs at Pamukkale and Karahayit are 33 to 55°C (Gökgöz, 1998; Kele *et al.*, 2011). The similar carbon and oxygen isotope compositions of these two areas (Fig. 12) imply that the origin of CO_2 is probably similar. The high $\delta^{13}C$ values of the travertines around Pamukkale have been attributed to the contribution of heavy CO_2 released during thermometamorphic decarbonation of carbonate basement rocks (i.e. Triassic–Jurassic marble, Miocene lacustrine limestone) (Özler, 2000; Şimşek *et al.*, 2000; Kele *et al.*, 2011). The $\delta^{13}C$ values of Aksaz show a more uniform distribution in comparison with Pamukkale (Fig. 12). However, the high $\delta^{13}C$ values at Pamukkale (Fig. 12) are caused by the downslope ^{13}C increase due to CO_2 degassing along the discharge aprons (Kele *et al.*, 2011). The similar stable isotopic compositions of the fossil and recent travertines in the Aksaz area indicate that the geothermal system remained nearly constant throughout the late Quaternary to the present.

CONCLUSIONS

Late Quaternary travertine deposits, south of the Uşak geothermal field in western Turkey, occur in a fluvial setting along the north-west and north-east trending stream valleys that were established on tectonic lines (for example, faults and fractures). The present thermal springs, saturated with respect to calcite, with temperatures of 32 to 38°C, are aligned along the stream bed. The springs of Na–Ca–SO_4–HCO_3 type are submerged by running stream waters in the wet season, whereas they are exposed in the dry season.

Based on the various facies combinations described, three travertine facies associations have been identified: (i) waterfall facies association; (ii) slope facies association; and (iii) pool facies association. The waterfall and slope facies associations form from thermal springs located in the hilly topography, whereas the horizontally bedded and laterally extensive travertines of the pool facies association, which are dominated by

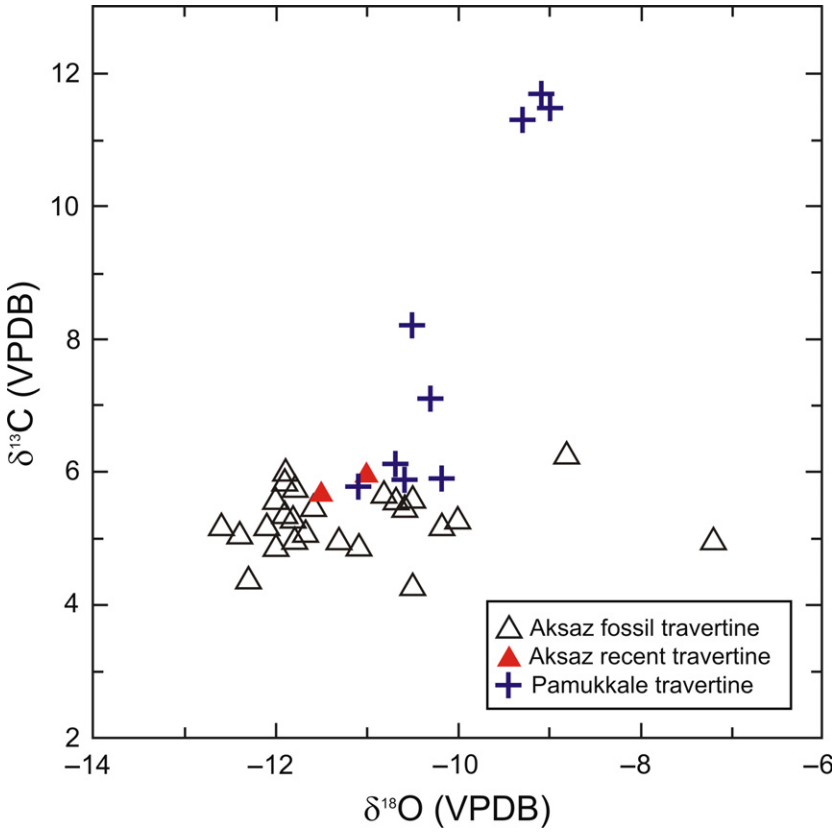

Fig. 12. Comparison of the $\delta^{13}C$ and $\delta^{18}O$ values of Aksaz and Pamukkale travertines. The stable isotope composition of the recent travertines collected in or close to the spring vents at Aksaz and Pamukkale show similar values. The high $\delta^{13}C$ values at Pamukkale are caused by continuous CO_2 degassing downslope (Kele *et al.*, 2011).

the micritic facies, precipitate in the restricted pools or depressions (for example, floodplain) located in the expanded parts of the stream bed. Fluvial detrital deposits are more prominent in the lower portions of the travertine succession and decrease upwards. The fluvial model, already being used for tufa, is proposed here for the first time to explain travertine deposits precipitated from hot-water springs emerging along a narrow ephemeral stream valley. Travertine precipitation in the Aksaz area, ranging from 153 ka to 1·85 ka, is evident in interglacial periods (MIS 3 and MIS 1), as well as glacial periods (MIS 6). The younger generation of the travertine precipitates, adjacent to the bath ruins of the Roman period (1·85 ka) and the Uyuz thermal spring, are those located closer to the present stream bed.

High stable carbon isotope values up to 6·3‰ (VPDB) show that the Aksaz travertines have been precipitated from thermal waters that are rich in deep sourced heavy CO_2 released during thermometamorphic decarbonation of carbonate bedrocks. The temperatures of the palaeosprings were, in general, slightly higher than those of the current springs, but sometimes were significantly lower, possibly due to mixing with stream water.

ACKNOWLEDGEMENTS

This work has been financially supported by the Scientific and Technological Research Council of Turkey - TÜBİTAK (grant 108Y016 to MÖ, AG, MOB, AK, MH, TA and ZÖ). Funding was also provided by Taiwan ROC NSC grants (NSC 99-2628-M-002-012, 100-2116-M-002-009 and 100-2116-M-002-009 to CCS). Yaşar Leblebici provided valuable field assistance. The authors are grateful to Chief Editor Tracy Frank, Associate Editor Enrico Capezzuoli and the anonymous referees for their critical reviews. Martyn Pedley, Brian Jones and Halim Mutlu are thanked for their helpful suggestions and linguistic revisions.

REFERENCES

Akkuş, İ., **Akıllı, H.**, **Ceyhan, S.**, **Dilemre, A.** and **Tekin, Z.** (2005) *Türkiye Jeotermal Kaynakları Envanteri. Envanter Serisi-201*. Maden Tetkik ve Arama Genel Müdürlüğü, Ankara, Turkey, 849 pp.

Alçiçek, H., **Varol, B.** and **Özkul, M.** (2005) Pisolith formation in self-built channel travertine, Pamukkale, Denizli, Western Turkey. In: *Proceedings of the 1st International Symposium on Travertine* (Eds M. Özkul, S. Yagiz and B. Jones), pp. 62–69. Kozan Ofset Matbaacilik San. Tic. Ltd. Sti, Ankara.

Altunel, E. and **Hancock, P.L.** (1993) Morphology and structural setting of Quaternary Travertines at Pamukkale, Turkey. *Geol. J.*, **28**, 335–346.

Andrews, J.E., **Pedley, H.M.** and **Dennis, P.F.** (2000) Palaeoenvironmental records in Holocene Spanish tufas: a stable isotope approach in search of reliable climatic archives. *Sedimentology*, **47**, 961–978.

Anzalone, E., **Ferreri, V.**, **Sprovieri, M.** and **D'Argenio, B.** (2007) Travertines as hydrologic archives: the case of the Pontecagnano deposits (southern Italy). *Adv. Water Resour.*, **30**, 2159–2175.

Arenas, C., **Gutierrez, F.**, **Osácar, C.** and **Sancho, C.** (2000) Sedimentology and geochemistry of fluvio-lacustrine tufa deposits controlled by evaporate solution subsidence in the central Ebro Depression, NE Spain. *Sedimentology*, **47**, 883–909.

Arenas-Abad, C., **Vázquez-Urbez, M.**, **Pardo-Tirapu, G.** and **Sancho-Marcén, C.** (2010) Fluvial and associated carbonate deposits. In: *Carbonates in Continental Settings: Facies, Environments, and Processes* (Eds A.M. Alonso Zarza and L.H. Taner), *Dev. Sedimentol.*, **61**, 133–175.

Bozkurt, E. and **Park, R.G.** (1994) Southern Menderes Massif: an incipient metamorphic core complex in western Anatolia, Turkey. *J. Geol. Soc. London*, **151**, 213–216.

Brogi, A. and **Capezzuoli, E.** (2009) Travertine deposition and faulting: the fault-related travertine fissure-ridge at Terme S. Giovanni, Terme, Italy. *Int. J. Earth Sci.*, **98**, 931–947.

Capezzuoli, E. and **Gandin, A.** (2005) Facies distribution and microfacies of thermal-spring travertine from Tuscany. In: *Proceedings of the 1st International Symposium on Travertine* (Eds. M. Özkul, S. Yagiz and B. Jones), pp. 43–49. Kozan Ofset Matbaacilik Sanayi Ticaret Limited şirketi. Ankara.

Capezzuoli, E., **Gandin, A.** and **Pedley, H.M.** (2013) Decoding tufa and travertine (fresh water carbonates) in the sedimentary record: The state of the art. *Sedimentology*. doi:10.1111/sed.12075.

Carthew, K.D., **Taylor, M.P.** and **Drysdale, R.N.** (2003) Are current models of tufa sedimentary environments applicable to tropical systems? A case study from the Gregory River. *Sed. Geol.*, **162**, 199–218.

Carthew, K.D., **Taylor, M.P.** and **Drysdale, R.N.** (2006) An environmental model of the fluvial tufas of the seasonally humid tropics, northern Australia. *Geomorphology*, **73**, 78–100.

Chafetz, H.S. and **Folk, R.L.** (1984) Travertines: depositional morphology and the bacterially constructed constituents. *J. Sed. Petrol.*, **54**, 289–316.

Chafetz, H.S., **Rush, P.F.** and **Utech, N.M.** (1991) Microenvironmental controls on mineralogy and habit of $CaCO_3$ precipitates: an example from an active travertine system. *Sedimentology*, **38**, 107–126.

Cheng, H., **Edwards, R.L.**, **Hoff, J.**, **Gallup, C.D.**, **Richards, D.A.** and **Asmersom, Y.** (2000) The half-lives of uranium–234 and thorium–230. *Chem. Geol.*, **169**, 17–33.

Cole, J.M., **Rasbury, E.T.**, **Montañez, I.P.**, **Pedone, V.A.**, **Lanzirotti, A.** and **Hanson, G.N.** (2004) Petrographic and trace element analysis of uranium-rich tufa calcite, middle Miocene Barstow Formation, California, USA. *Sedimentology*, **51**, 433–453.

Coleman, M.L., **Sheppard, T.J.**, **Durham, J.J.**, **Rouse, J.E.** and **Moore, G.R.** (1982) Reduction of water with zinc for hydrogen isotope analysis. *Anal. Chem.*, **54**, 993–995.

Coplen, T.B. (2007) Calibration of the calcite-water oxygen-isotope geothermometer at Devils Hole, Nevada, a natural laboratory. *Geochim. Cosmochim. Acta*, **71**, 3948–3957.

Coplen, T.B., **Wildman, J.D.** and **Chen, J.** (1991) Improvements in the gaseous hydrogen – water equilibration technique for hydrogen isotope-ratio analysis. *Anal. Chem.*, **63**, 910–912.

Craig, H. (1961) Isotopic variation in meteoric waters. *Science*, **133**, 1702–1703.

Davraz, A. (2008) Hydrogeochemical and hydrogeological investigations of thermal waters in the Usak Area (Turkey). *Environ. Geol.*, **54**, 615–628.

D'Argenio, B. and **Ferreri, V.** (2004) Travertines as self regulating carbonate systems. Evolutionary trends and classification. *Földtani Közlöny*, **1343**, 209–218.

De Filippis, L., **Faccenna, C.**, **Billi, A.**, **Anzalone, E.**, **Brilli, M.**, **Özkul, M.**, **Soligo, M.**, **Tuccimei, P.** and **Villa, M.** (2012) Growth of fissure ridge travertines from geothermal springs of Denizli Basin, western Turkey. *Geol. Soc. Am. Bull.*, **124**, 1629–1645.

Demény, A. (1995) H isotope fractionation due to hydrogen–zinc reactions and its implications on D/H analysis of water samples. *Chem. Geol.*, **121**, 19–25.

Epstein, S. and **Mayeda, T.** (1953) Variation of ^{18}O content of waters from natural sources. *Geochim. Cosmochim. Acta*, **4**, 89–103.

Ercan, T., **Dincel, A.**, **Metin, S.**, **Turkecan, A.** and **Günay, E.** (1978) Geology of the Neogene basins in Usak region. *Bull. Geol. Soc. Turk.*, **21**, 97–106. (in Turkish with English abstract).

Ercan, E., **Türkecan, A.**, **Dinçel, A.** and **Günay, E.** (1983) Geology of Kula-Selendi (Manisa) area. *Geol. Eng.*, **17**, 3–28. (in Turkish with English abstract).

Ersoy, E. and **Helvacı, C.** (2007) Stratigraphy and geochemical features of the Early Miocene bimodal (ultrapotassic and calc-alkaline) volcanic activity within the NE-trending Selendi Basin, Western Anatolia, Turkey. *Turk. J. Earth Sci.*, **16**, 117–139.

Ersoy, E.Y., **Helvacı, C.**, **Sözbilir, H.**, **Erkül, F.** and **Bozkurt, E.** (2008) A geochemical approach to Neogene–Quaternary volcanic activity of western Anatolia: an example of episodic bimodal volcanism within the Selendi Basin, Turkey. *Chem. Geol.*, **255**, 265–282.

Ersoy, E.Y., **Helvacı, C.** and **Palmer, M.R.** (2010) Mantle source characteristics and melting models for the early-middle Miocene mafic volcanism in Western Anatolia: implications for enrichment processes of mantle lithosphere and origin of K-rich volcanism in post-collisional settings. *J. Volcanol. Geoth. Res.*, **198**, 112–128.

Faccenna, C., **Soligo, M.**, **Bili, A.**, **De Filippis, L.**, **Funiciello, R.**, **Rossetti, C.** and **Tuccimei, P.** (2008) Late Pleistocene depositional cycles of the Lapis Tiburtinus travertine (Tivoli, Central Italy): possible influence of climate and fault activity. *Global Planet. Change*, **63**, 299–308.

Folk, R.L. and **Chafetz, H.S.** (1983) Pisoliths (pisoliths) in Quaternary travertines of Tivoli, Italy. In: *Coated Grains*, pp. 474–487. (Ed T.M. Peryt), Springer-Verlag, Berlin.

Folk, R.L., **Chafetz, H.S.** and **Tiezzi, P.A**. (1985) Bizarre forms of depositional and diagenetic calcite in hot-spring travertines, central Italy. In: *Carbonate Cements* (Eds. N. Schneidermann and M. Harris), *SEPM Spec. Publ.*,**36**, 349–369.

Ford, T.D. and **Pedley, H.M.** (1996) A review of tufa and travertine deposits of the world. *Earth-Sci. Rev.*, **41**, 117–175.

Fouke, B.W., **Farmer, J.D.**, **Des Marais, D.J.**, **Pratt, L.**, **Sturchio, N.C.**, **Burns, P.C.** and **Discipulo, M.K.** (2000) Depositional facies and aqueous-solid geochemistry of travertinedepositing hot springs (Angel Terrace, Mammoth Hot Springs, Yellowstone National Park, U.S.A). *J. Sed. Res.*, **70**, 565–585.

Fouke, B.W. (2011) Hot-spring Systems Geobiology: abiotic and biotic influences on travertine formation at Mammoth Hot Springs, Yellowstone National Park, USA. *Sedimentology*, **58**, 170–219.

Fournier, R.O. (1977) Chemical geothermometers and mixing models for geothermal systems. *Geothermics*, **5**, 41–50.

Friedman, I. and **O'Neil, J.R**. (1977) Compilation of stable isotope fractionation factors of geochemical interest. In: *Data of Geochemistry*, 6th edition (Ed. M. Fleischer), *Geol. Surv. Prof. Paper*, **440-KK**, 61.

Gessner, K., **Ring, U.**, **Christopher, J.**, **Hetzel, R.**, **Passchier, C.W.** and **Güngör, T.** (2001) An active bivergent rolling-hinge detachment system: central Menderes metamorphic core complex in western Turkey. *Geology*, **29**, 611–614.

Gierlowski-Kordesch, E.H. (2010) Lacustrine carbonates. In: *Carbonates in Continental Settings: Facies, Environments and Processes* (Eds A.M. Alonso-Zarza and L.H. Tanner), *Dev. Sedimentol.*, **61**, 1–102.

Guo, L. and **Riding, R.** (1998) Hot-spring travertine facies and sequences, Late Pleistocene Rapolano Terme, Italy. *Sedimentology*, **45**, 163–180.

Gökgöz, A. (1998) Geochemistry of the Kızıldere-Tekkehamam-Buldan-Pamukkale Geothermal Fields. United Nations University, Geothermal Training Programme, Reports, 115–156. Reykjavik, Iceland.

Hancock, P.L., **Chalmers, R.M.L.**, **Altunel, E.** and **Cakir, Z.** (1999) Travitonics: using travertines in active fault studies. *J. Struct. Geol.*, **21**, 903–916.

Hetzel, R., **Ring, U.**, **Akal, C.** and **Troesch, M.** (1995) Miocene NNE directed extensional unroofing in the Menderes Massif, southwestern Turkey. *J. Geol. Soc. London*, **152**, 639–654.

Innocenti, F., **Agostini, S.**, **Di Vincenzo, G.**, **Doglioni, C.**, **Manetti, P.**, **Savaşçın, M.Y.** and **Tonarini, S.** (2005) Neogene and Quaternary volcanism in Western Anatolia: magma sources and geodynamic evolution. *Mar. Geol.*, **221**, 397–421.

Jaffey, A.H., **Flynn, K.F.**, **Glendenin, L.E.**, **Bentley, W.C.** and **Essling, A.M.** (1971) Precision measurement of half-lives and specific activities of U-235 and U-238. *Phys. Rev.*, **4**, 1889–1906.

Jones, B. and **Renaut, R.W.** (1995) Noncrystallographic dendrites from hot-spring deposits at Lake Bogoria, Kenya. *J. Sed. Res.*, **65**, 154–169.

Jones, B. and **Renaut, R.W.** (2008) Cyclic development of large, complex calcite dendrite crystals in the Clinton travertine, Interior British Columbia, Canada. *Sed. Geol.*, **203**, 17–35.

Jones, B. and **Renaut, R.W**. (2010) Calcareous spring deposits in continental settings. In: *Carbonates in Continental Settings: Facies, Environments, and Processes* (Eds A.M. Alonso Zarza and L.H. Taner), *Dev. Sedimentol.*, **61**, 177–204.

Jones, B., **Renaut, R.W.**, **Owen, R.B.** and **Torfason, H.** (2005) Growth patterns and implications of complex dendrites in calcite travertines from Lýsuhóll, Snæfellsnes, Iceland. *Sedimentology*, **52**, 1277–1301.

Kele, S., **Demény, A.**, **Siklósy, Z.**, **Németh, T.**, **Mária, T.** and **Kovács, M.B.** (2008) Chemical and stable isotope

compositions of recent hot-water travertines and associated thermal waters, from Egerszalók, Hungary: depositional facies and non-equilibrium fractionations. *Sed. Geol.*, **211**, 53–72.

Kele, S., **Özkul, M.**, **Fórizs, I.**, **Gökgöz, A.**, **Baykara, M.O.**, **Alçiçek, M.C.** and **Németh, T.** (2011) Stable isotope geochemical and facies study of Pamukkale travertines: new evidences of low-temperature non-equilibrium calcite-water fractionation. *Sed. Geol.*, **238**, 191–212.

Kendall, C. and **Coplen, T.B.** (1985) Multisample conversion of water to hydrogen by zinc for stable isotope determination. *Anal. Chem.*, **57**, 1437–1440.

Kim, S.-T. and **O'Neil, J.R.** (1997) Equilibrium and nonequilibrium oxygen isotope effects in synthetic carbonates. *Geochim. Cosmochim. Acta*, **61**, 3461–3475.

Martín-Algarra, A., **Martín - Martín, M.**, **Andreo, B.**, **Julià, R.** and **González-Gómez, C**. (2003) Sedimentary patterns in perched spring travertines near Granada (Spain) as indicators of the palaeohydrological and palaeoclimatological evolution of a karst massif. *Sed. Geol.*, **161**, 217–228.

McCrea, J.M. (1950) On the isotopic chemistry of carbonates and a paleotemperature scale. *J. Chem. Phys.*, **18**, 849–857.

Özkul, M., **Varol, B.** and **Alçiçek, M.C.** (2002) Depositional environments and petrography of the Denizli travertines. *Bull. Mineral Res. Explor.*, **125**, 13–29.

Özkul, M., **Gökgöz, A.** and **Horvatinčić, N.** (2010) Depositional properties and geochemistry of Holocene perched springline tufa deposits and associated spring waters: a case study from the Denizli province, Western Turkey. In: *Tufas and Speleothems: Unravelling the Microbial and Physical Controls*, pp. 245–262. (Eds H.M. Pedley and M. Rogerson), The Geological Society, London.

Özkul, M., **Kele, S.**, **Gökgöz, A.**, **Shen, C.C.**, **Jones, B.**, **Baykara, M.O.**, **Fórizs, I.**, **Németh, T.**, **Chang, Y.-W.** and **Alçiçek, M.C.** (2013) Comparison of the Quaternary travertine sites in the Denizli Extensional Basin based on their depositional and geochemical data. *Sed. Geol.*, **294**, 179–204.

Özler, H.M. (2000) Hydrogeology and geochemistry in the Curuksu (Denizli) hydrothermal field, western Turkey. *Environ. Geol.*, **39**, 1169–1180.

Parkhurst, D.L. and **Appelo, C.A.J**. (1999) User's guide to PHREEQC (Version 2 –A) Computer program for speciation, batch-reaction, one-dimensional transport, and inverse geochemical calculations. US Geological Survey Water-Resources Investigations, Report 99–4259.

Pedley, H.M. (1990) Classification and environmental models of cool freshwater tufas. *Sed. Geol.*, **68**, 143–154.

Pedley, H.M. (2009) Tufas and travertines of the Mediterranean region: a testing ground for freshwater carbonate concepts and developments. *Sedimentology*, **56**, 221–246.

Pedley, H.M., **Ordonez, S.**, **Gonzales-Martin, J.A.** and **Garcia Del Cura, M.A.** (2003) Sedimentology of Quaternary perched springline and paludal tufas: criteria for recognition, with examples from Guadalajara Province, Spain. *Sedimentology*, **50**, 23–44.

Pentecost, A. (2005) *Travertine*. Springer Verlag, Berlin, 446 pp.

Prosser, S.J. and **Scrimgeour, C.M.** (1995) High-precision determination of $^{2}H/^{1}H$ in H_2 and H_2O by continuous-flow isotope ratio mass spectrometry. *Anal. Chem.*, **67**, 1992–1997.

Purvis, M., **Robertson, A.** and **Pringle, M.** (2005) 40Ar–39Ar dating of biotite and sanidine in tuffaceous sediments and related intrusive rocks: implications for the Early Miocene evolution of the Gördes and Selendi basins, W Turkey. *Geodin. Acta*, **18**, 239–253.

Rainey, D.K. and **Jones, B.** (2009) Abiotic versus biotic controls on the development of the Fairmont Hot Springs carbonate deposit, British Columbia, Canada. *Sedimentology*, **56**, 1832–1857.

Renaut, R.W., **Owen, R.B.**, **Jones, B.**, **Tiercelin, J-J.**, **Corinne, T.**, **Ego, J.K.** and **Konhauser, K.O**. (2013) Impact of lake-level changes on the formation of thermogene travertine in continental rifts: evidence from Lake Bogoria, Kenya Rift Valley. *Sedimentology*, **60**, 428–468.

Richter, D.V. and **Besenecker, H.** (1983) Subrecent high-Sr aragonite ooids from hot springs near Tekke Ilica (Turkey). In: *Coated Grains*, pp. 154–162. (Ed T.M. Perty), Springer-Verlag, Berlin.

Sant'Anna, L.G., **Riccomini, C.**, **Rodrigues-Francisco, B.H.**, **Sial, A.N.**, **Carvalho, M.D.** and **Moura, C.A.V.** (2004) The Paleocene travertine system of the Itaboraı′ basin, Southeastern Brazil. *J. S. Am. Earth Sci.*, **18**, 11–25.

Seyitoğlu, G. (1997) Late Cenozoic tectono-sedimentary development of Selendi and Uşak-Güre basins: a contribution to the discussion on the development of eastwest and north-trending basins in western Turkey. *Geological Magazine*, **134**, 163–175.

Seyitoğlu, G., **Anderson, D.**, **Nowell, G.** and **Scott, B.C.** (1997) The evolution from Miocene potassic to Quaternary sodic magmatism in western Turkey: implications for enrichment processes in the lithospheric mantle. *J. Volcanol. Geoth. Res.*, **76**, 127–147.

Seyitoğlu, G., **Alçiçek, M.C.**, **Işık, V.**, **Alçiçek, H.**, **Mayda, S.**, **Varol, B.**, **Yılmaz, D.** and **Esat, K.** (2009) The stratigraphical position of Kemiklitepe fossil locality (Eşme, Uşak) revised: Implications for the Late Cenozoic sedimentary basin development and extensional tectonics in western Turkey. *Neues Jahrbuch fur Geologie und Palaontologie-Abhandlungen*, **251**, 1–15.

Shen, C.-C., **Edwards, R.L.**, **Cheng, H.**, **Dorale, J.A.**, **Thomas, R.B.**, **Moran, S.B.**, **Weinstein, S.E.** and **Hirschmann, M.** (2002) Uranium and thorium isotopic and concentration measurements by magnetic sector inductively coupled plasma mass spectrometry. *Chem. Geol.*, **185**, 165–178.

Shen, C.-C., **Cheng, H.**, **Edwards, R.L.**, **Moran, S.B.**, **Edmonds, H.N.**, **Hoff, J.A.** and **Thomas, R.B.** (2003) Measurement of attogram quantities of ^{231}Pa in dissolved and particulate fractions of seawater by isotope dilution thermal ionization mass spectroscopy. *Anal. Chem.*, **75**, 1075–1079.

Shen, C.-C., **Li, K.-S.**, **Sieh, K.**, **Natawidjaja, D.**, **Cheng, H.**, **Wang, X.**, **Edwards, R.L.**, **Lam, D.D.**, **Hsieh, Y.-T.**, **Fan, T.-Y.**, **Meltzner, A.J.**, **Taylor, F.W.**, **Quinn, T.M.**, **Chiang, H.-W.** and **Kilbourne, K.H.** (2008) Variation of initial $^{230}Th/^{232}Th$ and limits of high precision U-Th dating of shallow-water corals. *Geochim. Cosmochim. Acta*, **72**, 4201–4223.

Shen, C.-C., **Wu, C.-C.**, **Cheng, H.**, **Edwards, R.L.**, **Hsieh, Y.-T.**, **Gallet, S.**, **Chang, C.-C.**, **Li, T.-Y.**, **Lam, D.D.**, **Kano, A.**, **Hori, M.** and **Spötl, C.** (2012) High-precision and high-resolution carbonate ^{230}Th dating by MC-ICP-MS with SEM protocols. *Geochim. Cosmochim. Acta*, **99**, 71–86.

Sierralta, M., **Kele, S.**, **Melcher, F.**, **Hambach, U.**, **Reinders, J.**, **van Geldern, R.** and **Frechen, M.** (2010) Uranium-Series Dating of Travertine from Süttő: Implications for

Reconstruction of Environmental Change in Hungary. *Quatern. Int.*, **222**, 178–193.

Spötl, C. and **Vennemann, T.W.** (2003) Continuous-flow isotope ratio mass spectrometric analysis of carbonate minerals. *Rapid Commun. Mass Spectrom.*, **17**, 1004–1006.

Şimşek, Ş. (2003) Hydrogeological and isotopic survey of geothermal fields in the Büyük Menderes graben, Turkey. *Geothermics*, **32**, 669–678.

Şimşek, Ş., **Günay, G.**, **Elhatip, H.** and **Ekmekci, M.** (2000) Environmental protection of geothermal waters and travertines at Pamukkale, Turkey. *Geothermics*, **29**, 557–572.

Taylor, S.R. and **McLennan, S.M.** (1995) The geochemical evolution of the continental crust. *Rev. Geophys.*, **33**, 241–265.

Turner, E.C. and **Jones, B.** (2005) Microscopic calcite dendrites in cold-water tufa: implications for nucleation of micrite and cement. *Sedimentology*, **52**, 1043–1066.

Uysal, I.T., **Feng, Y.**, **Zhao, J.**, **Altunel, E.**, **Weatherley, D.**, **Karabacak, V.**, **Cengiz, O.**, **Golding, S.D.**, **Lawrence, M.G.** and **Collerson, K.D.** (2007) U-Series dating and geochemical tracing of late Quaternary travertine in co-seismic fissures. *Earth Planet. Sci. Lett.*, **257**, 450–462.

Uysal, I.T., **Feng, Y.**, **Zhao, J.**, **Işık, V.**, **Nuriel, P.** and **Golding, S.D.** (2009) Hydrothermal CO_2 degassing in seismically active zones during the late Quaternary. *Chem. Geol.*, **265**, 442–454.

Van Noten, K., **Claes, H.**, **Soete, J.**, **Foubert, A.**, **Özkul, M.** and **Swennen, R.** (2013) Fracture networks and strike–slip deformation along reactivated normal faults in Quaternary travertine deposits, Denizli Basin, western Turkey. *Tectonophysics*, **588**, 154–170.

Vázquez-Urbez, M., **Arenas, C.** and **Pardo, G.** (2012) A sedimentary facies model for stepped, fluvial tufa systems in the Iberian Range (Spain): the Quaternary Piedra and Mesa valleys. *Sedimentology*, **59**, 502–526.

Viles, H.A., **Taylor, M.P.**, **Nicoll, K.** and **Neumann, S.** (2007) Facies evidence of hydroclimatic regime shifts in tufa depositional sequences from the arid Naukluft Mountains, Namibia. *Sed. Geol.*, **195**, 39–53.

Manuscript received 3 June 2012; revision 08 November 2012; revision accepted 14 November 2013